

Problems and issues in laser-arc hybrid welding

B. Ribic, T. A. Palmer and T. DebRoy*

Hybrid welding, using the combination of a laser and an electrical arc, is designed to overcome problems commonly encountered during either laser or arc welding such as cracking, brittle phase formation and porosity. When placed in close contact with each other, the two heat sources interact in such a way as to produce a single high intensity energy source. This synergistic interaction of the two heat sources has been shown to alleviate problems commonly encountered in each individual welding process. Hybrid welding allows increased gap tolerances, as compared to laser welding, while retaining the high weld speed and penetration necessary for the efficient welding of thicker workpieces. A number of simultaneously occurring physical processes have been identified as contributing to these unique properties obtained during hybrid welding. However, the physical understanding of these interactions is still evolving. This review critically analyses the recent advances in the fundamental understanding of hybrid welding processes with emphases on the physical interaction between the arc and laser and the effect of the combined arc/laser heat source on the welding process. Important areas for further research are also identified.

Keywords: Hybrid welding, Laser welding, Arc welding, Heat transfer, Fluid flow, Microstructure, Review

List of symbols and acronyms

a	coefficient in the surface tension pressure term	h	depth of keyhole (mm)
A	area of the transverse weld cross-section (mm^2)	H	heat input per unit length (J mm^{-1})
\mathbf{B}	magnetic flux ($\text{kg s}^{-2} \text{A}^{-1}$)	HAZ	heat affected zone
c	molar concentration of vapour inside keyhole (mol cm^{-3})	HCP	hexagonal close packed
C	concentration of surface active elements (wt-%)	H_f	latent heat of fusion (J kg^{-1})
C_p	heat capacity or specific heat ($\text{J kg}^{-1} \text{K}^{-1}$)	I	arc current (A)
DCEN	direct current electrode negative	I_a	attenuated laser beam intensity (W)
DCEP	direct current electrode positive	I_m	imaginary portion of the complex refractive index
D_{LA}	horizontal distance between laser focal point and arc electrode tip	I_o	initial laser beam intensity (W)
dT/dy	spatial temperature gradient on the weld pool surface (K mm^{-1})	J	flux of evaporating particles in keyhole ($\text{mol cm}^{-2} \text{s}^{-1}$)
E_A	attenuated incident radiation (W)	\mathbf{J}_c	current density (A m^{-2})
f	distribution factor	k_e	extinction coefficient
F_b	buoyancy force (N m^{-3})	k	thermal conductivity ($\text{W m}^{-1} \text{K}^{-1}$)
\mathbf{F}_{emf}	Lorentz or electromagnetic force (N m^{-3})	L	characteristic length (half of the weld pool width) (mm)
g	acceleration due to gravity (m s^{-2})	L_p	length of the plasma (mm)
GMA	gas metal arc	L_R	characteristic length of the weld pool (mm)
GMAW	gas metal arc welding	m	complex refractive index
GTA	gas tungsten arc	n	refractive index
GTAW	gas tungsten arc welding	N	number density of scattering particles (no./mm)
		Nd:YAG	neodymium:yttrium aluminium garnet
		P	incident heat source power (W)
		P_d	power density (W mm^{-2})
		Pe	Peclet number
		P_r	recoil pressure (Pa)
		P_v	vapour pressure (Pa)
		P_n	power or nominal power (W)
		P_t	total power of the heat source (W)

Department of Materials Science and Engineering, The Pennsylvania State University, University Park, PA 16802, USA

*Corresponding author, email rtd1@psu.edu

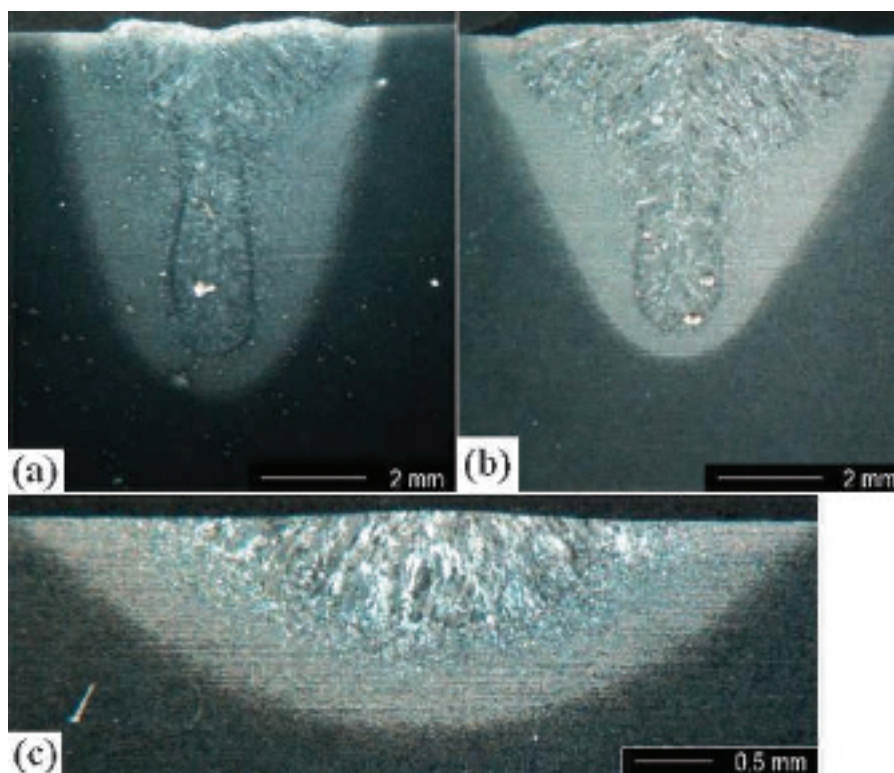
P_γ	pressure due to surface tension effects (Pa)
Q_A	amount of attenuation due to absorption
Q_i	heat transfer rate (kW)
Q_m	melting rate (kW)
Q_o	welding process nominal power (kW)
Q_s	amount of attenuation due to scattering
r	radial distance from the axis of the heat source (mm)
r_b	radius of heat source (mm)
Re_m	magnetic Reynolds number
Re_m/Re_s	ratio of magnetic to surface tension forces
Re_s	surface tension Reynolds number
r_k	keyhole radius (mm)
r_p	average radius of particles in plasma (mm)
T	temperature (K)
T_m	melting temperature of a material (K)
T_o	ambient temperature (K)
T_{ref}	arbitrary selected reference temperature (K)
U	characteristic velocity of the liquid metal (mm s^{-1})
v	welding velocity or speed (mm s^{-1})
v_v	metal vapour velocity (m s^{-1})
Yb	ytterbium
z	distance over which laser beam attenuation occurs (mm)
α	thermal diffusivity ($\text{m}^2 \text{s}^{-1}$)
β	thermal expansion coefficient (K^{-1})
γ	surface tension (N m^{-1})
$\partial\gamma/\partial T$	temperature coefficient of surface tension ($\text{N m}^{-1} \text{K}^{-1}$)
ΔP	pressure gradient due to vapour flow out of keyhole (Pa)

ΔT	difference between the weld pool peak temperature and the solidus temperature (K)
η_h	heat transfer efficiency (%)
η_m	melting efficiency (%)
λ	laser beam wavelength (nm)
μ	liquid viscosity (Pa s)
μ_a	absorption coefficient (mm^{-1})
μ_m	magnetic permeability (H m^{-1} or N A^{-2})
μ_v	viscosity of the metal vapour in the keyhole (Poise)
ρ	density (kg m^{-3})
ρ_l	density of liquid material (kg m^{-3})
ρ_v	evaporating gas particle density (kg m^{-3})
τ	Marangoni stress (N m^{-2})

Introduction

Hybrid welding combines laser and arc sources in such a way that the benefits of both welding processes are obtained.¹⁻⁵ As a result, hybrid welding produces weld pools that are wider than laser welds and deeper than arc welds made with the same laser and arc welding parameters respectively.⁶⁻¹⁸ Differences in the weld geometries produced by autogenous laser, hybrid and arc welding are shown in Fig. 1. The arc weld shown in Fig. 1c is shallower than both the laser and hybrid weld pools¹⁹ shown in Fig. 1a and b respectively. The width of the hybrid weld is comparable to that of the arc weld.

Hybrid welding also provides enhanced productivity and capabilities in excess of what can be achieved by either laser or arc welding alone.^{10,11,19} For example, hybrid welds have shown a reduction in the presence of



1 Weld cross-sections of a laser, b hybrid and c arc welded A131 structural steel specimens. For the laser and hybrid welds,¹⁹ the laser power is 4.5 kW. The arc current and voltage are 191 A and 11 V respectively, for the arc weld, and 190 A and 12.3V for the hybrid weld. The welding speed is 0.51 m min^{-1} for all three welds¹⁹

brittle phases,^{20–22} cracks,²³ thermal distortion^{12,24,25} and porosity^{13,26–28} compared to both laser and arc welds. One of its main advantages involves the ability to bridge gaps between workpieces in excess of that possible during laser welding.^{19,29–35} Finally, the combination of the laser and the arc in hybrid welding allows for the use of significantly higher welding velocities to achieve deeper penetrations than possible with arc welding alone.^{36–40} This enhanced capability allows for full penetration welds to be achieved in a single pass, thus removing the need for additional passes.^{10,41–45}

In addition to these differences in weld pool geometry, there are a number of other important differences in the welds produced by the three processes. Table 1 compares the properties of arc, laser and hybrid welds with respect to gap bridging, formation of residual stresses and distortion, process productivity, cracking propensity, cooling rate, weld penetration and arc stability. These properties are important considerations when joining large and thick components. Overall, the hybrid welding process is able to take advantage of the benefits of laser and arc welding, resulting in a process that can produce wide and deep welds in a single pass with low distortion and residual stress.^{46–49}

The benefits of the hybrid welding process mainly arise out of the physical interaction of the two heat sources.^{1,50–53} This interaction is a highly complex physical process in which metal vapour generated by the laser can vastly affect the electrical and thermal conductivity of the arc plasma and the behaviour of the arc column. The interaction of the two heat sources greatly affects the resulting weldment properties.^{51,52,54,55} One means by which the interaction between the heat sources can be altered involves the separation between the laser and the arc, resulting in either hybrid or tandem welding conditions. Recent work by Mahrle and Beyer¹¹ has tried to establish a clear delineation between the two welding processes. Based on this work, hybrid welding can be defined as the

condition when the laser and arc are situated closely enough together that their plasma phases interact with each other. Commonly, the heat sources are separated by a distance of 5 mm or less, depending on the welding process parameters and the material.^{19,42,56} Tandem welding occurs when the laser and arc are separated by a distance at which no plasma interaction occurs.

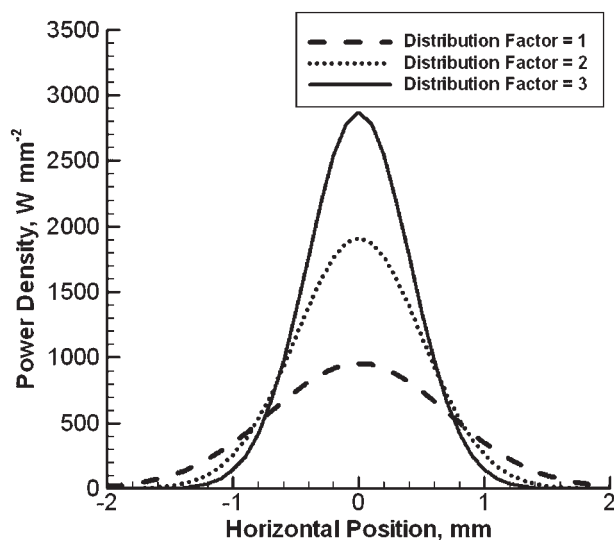
The current understanding of hybrid welding is primarily based on empirical observations, with much of the existing literature covering the use of hybrid welding to join a range of materials. Currently, hybrid welding is restricted to specific applications, predominantly involving the joining of thick section plain carbon steels. In order for the application space for hybrid welding to be expanded and the process optimised for its current applications, knowledge of the mechanisms governing the physical processes in hybrid welding must be better understood. This review analyses the current scientific understanding of these underlying physical phenomena and mechanisms of hybrid welding. Particular attention is given to the interaction between the arc and laser and the effect of these two heat sources on energy absorption, heat transfer, fluid flow, the mechanisms of common defect formation, and the structure and properties of the welds. Based on the review of the current knowledge base, important areas for further research are also identified.

Physics of arc and laser processes

During welding, energy absorption by the workpiece affects the temperature profiles, solidification, microstructure, mechanical properties and geometry of the weld pool. In order to understand hybrid welding, it is important to examine the physics of the arc and laser welding processes separately. Although several reviews on the fundamentals of fusion welding are available in the literature,^{57–61} a brief critical assessment is presented here to aid in the understanding of the hybrid welding process.

Table 1 Comparison of arc, laser and hybrid welding processes

	Arc welding	Laser welding	Hybrid welding
Gap bridging	Wide fusion zone Use of filler metal Good gap bridging	Narrow fusion zone Poor gap bridging	Wide fusion zone Good gap bridging
Residual stress and distortion	High heat input per unit length High residual stress and distortion	Low heat input per unit length Low residual stress and distortion	Low heat input per unit length Low residual stress and distortion
Productivity	Low welding speed Low productivity	High welding speed High productivity	Relatively high welding speed High productivity
Cracking propensity	High propensity for solidification cracking	Formation of brittle phases Increased propensity for cracking	Reduced amounts of residual stress Low propensity for cracking
Cooling rate	Low cooling rate Prevents brittle phase formation	High cooling rates Relatively high amounts of porosity	Relatively low cooling rates Reduced amount of porosity
Weld penetration	Relatively shallow fusion zone Reduced penetration Multipass welding	High energy density Deep weld pool Single pass welding of thick sections	Relatively deep weld pool Single pass welding of thick sections
Arc stability	Reduced arc stability at higher welding speeds leads to humping	Keyhole instability	Interaction between laser and arc stabilises the arc



2 Power density as a function of horizontal position relative to the heat source symmetry axis with varying distribution factors for a 3 kW heat source. The effect of distribution factor on energy distribution shape and the size of the area affected by the heat source is shown. Laser heat sources tend to have energy distributions similar to the solid line ($f=3$), while electrical arc energy distributions are similar to the dashed line ($f=1$)

Role of power density distribution

The radius of the heat source and the power density distribution are important parameters in laser and arc welding. The power density of laser and arc sources can often be represented by a Gaussian distribution⁶²

$$P_d = \frac{fP_t}{\pi r_b^2} \exp\left(-\frac{fr^2}{r_b^2}\right) \quad (1)$$

where f is the distribution factor, P_t is the total power of the heat source, r_b is the radius of the heat source and r is the radial distance from the axis of the heat source. Figure 2 shows a plot of power density as a function of horizontal position relative to the heat source symmetry axis for various values of the distribution factor f . As the distribution factor increases, the energy becomes more focused, resulting in an increase in the peak temperature at the centre of the laser beam or arc. The typical power density distribution of a laser beam is characterised by a higher distribution factor than that of an arc and is represented in Fig. 2 by the solid line ($f=3$). With a distribution factor of 3, the laser has a higher peak power density than the arc distribution, which is represented by the dashed line with a distribution factor of 1.

The power density distribution describes the nature of the heat source that interacts with the workpiece and is important in predicting the weld pool geometry. For example, sharp and highly intense power density distributions produce a keyhole, resulting in a deep and narrow weld pool.^{63–67} Less intense laser power density distributions result in conduction mode welds which are nearly hemispherical in shape.^{63,68,69} Changes in the focus position of the laser also have an effect on the power density distribution. When the laser beam is positively defocused, the keyhole depth drops because of the divergent nature of the laser beam. On the other hand, when the laser beam is negatively defocused, the beam is convergent and the power density increases with

depth up to the focal point, which may result in increased keyhole depth depending upon the operating mode of the laser beam and depth of focus of the laser.^{3,30,33}

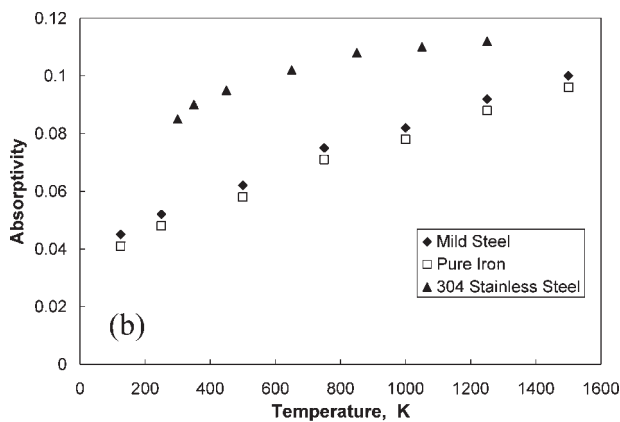
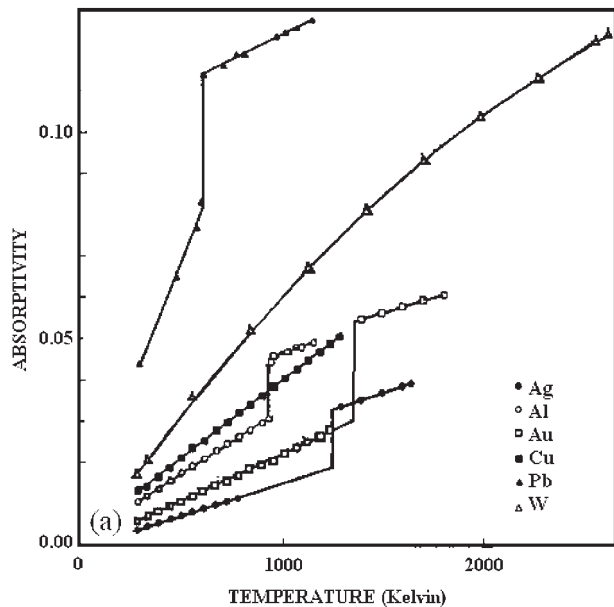
Absorption of arc and laser

In arc and laser welding, the workpiece absorbs only a portion of the total energy supplied by the heat source, depending on the material, the type of heat source and the process parameters.^{58,63,70,71} The amount of energy absorbed by the workpiece is expressed as the process efficiency, which takes into account the power density distribution of the heat source and selected thermo-physical properties, such as the thermal conductivity and specific heat of the material. The process parameters also influence process efficiency by directly affecting the power density distribution of the heat source or the heat input per unit length.

The type of heat source affects process efficiency through differences in the mechanisms of energy transfer. For an arc, energy absorption by the workpiece is affected by the manner in which the electrical circuit of the arc is arranged, the metal transfer mode, the shielding gas used and the workpiece material.^{14,29,62,63} Electrical arcs can be generated using direct (dc) or alternating current (ac).⁶² Depending upon the polarity of the electrical circuit, electrons are emitted or received at the electrode.⁶² Gas metal arc welding (GMAW) employs direct current electrode positive (DCEP) to avoid erratic metal transfer, while gas tungsten arc welding (GTAW) can operate using a direct or alternating current.⁶² The arrangement of the electrical circuit of the arc is more important for GTAW, while metal transfer mode is more important for GMAW.

The absorption of laser energy by the workpiece differs from the energy absorption of arcs and is affected by factors such as the laser wavelength, nature of the workpiece surface, joint geometry, and the size and nature of the plasma present above the weld pool.^{58,72–74} Figure 3a shows the dependence of absorptivity on temperature⁷² for several pure materials irradiated at a wavelength of 10.6 μm . As the temperature of the workpiece increases, absorptivity increases, and once a material melts, absorptivity increases significantly, resulting in the discontinuities shown in each curve. Upon melting, convection aids in the transport of heat in the molten weld pool. Figure 3b shows the absorptivity for mild steel,⁷⁵ AISI 304 stainless steel⁷³ and iron⁷⁵ as a function of temperature for a laser beam wavelength of 10.6 μm based on work by Duley⁷⁵ and Boyden and Zhang.⁷³ The absorptivity of mild steel is $\sim 9\%$ higher than that of iron and varies similarly as a function of temperature.⁷⁵ While the absorptivity of solid iron increases with temperature in a manner similar to other pure metals, 304 stainless steel shows much less variation in absorptivity over the same temperature range.

Absorption of infrared energy by metals depends on Fresnel absorption,^{63,76–78} which is simply defined as the conductive absorption by free electrons.⁷⁹ With Fresnel absorption, a portion of the laser energy is either reflected or absorbed by the workpiece. Reflected laser energy plays an important role inside the laser generated keyhole.^{65–67} When a plasma phase is present, a portion of the laser energy is absorbed by the plasma through inverse Bremsstrahlung absorption, while the remainder of the incident radiation is transmitted to the workpiece



3 a temperature dependence of absorptivity⁷² for pure Al, Ag, Au, Cu, Pb and W at a laser wavelength of 10.6 μm and b temperature dependence of absorptivity for mild steel,⁷⁵ AISI 304 stainless steel⁷³ and iron⁷⁵ at a laser wavelength of 10.6 μm

material.^{58,63,76,80} Inverse Bremsstrahlung absorption occurs when energy of the electric field induced by the laser is absorbed by the plasma via electron-ion collisions.⁸¹

When a keyhole forms during laser welding, the absorption efficiency of the laser increases greatly due to the multiple reflections of the laser beam within the keyhole.^{58,65-67} As a result, the energy from the laser is able to penetrate to a greater depth into the workpiece without changing the weld width, thus increasing the weld aspect ratio.^{50,82} Often in this case, a laser induced plasma forms and some laser energy is absorbed by the plasma phase formed within the keyhole. This condition is most often quantitatively described by the Beer-Lambert law given by⁵⁰

$$I_a = I_o \exp(-\mu_a L_p) \tag{2}$$

where I_a and I_o are the attenuated and the initial laser beam intensity respectively, μ_a is the absorption coefficient and L_p is the length of the plasma. Often the Beer-Lambert law is empirically modified depending upon the size of the particles which comprise the plasma, the nature of the interacting particles in the plasma and

the workpiece material. The Beer-Lambert law is redefined in the following relationship and is applicable for plasmas containing particles on the order of 20–50 nm in diameter⁷⁴

$$E_A = P \left[1 - \exp^{-(Q_s + Q_a)\pi r_p^2 N z} \right] \tag{3}$$

where E_A is the attenuated incident radiation in watts, P is the incident laser power, r_p is the average radius of the particles, N is the number density of the scattering particles, z is the distance over which attenuation of laser beam energy occurs, Q_s is the amount of attenuation due to scattering and Q_a is the amount of attenuation due to absorption.

For a shorter wavelength heat source, scattering will play a larger role in the laser beam attenuation.⁷⁴ The amount of attenuation due to scattering Q_s is inversely proportional to the fourth power of the wavelength of the laser heat source, as shown by the following relationship⁷⁴

$$Q_s = \frac{8}{3} \left(\frac{2\pi r}{\lambda} \right)^4 \left| \frac{m^2 - 1}{m^2 + 2} \right|^2 \tag{4}$$

where m is the complex refractive index ($m = n + k_e i$), n is the refractive index of the material and λ is the laser wavelength. The extinction coefficient k_e is simply the fraction of incident radiation lost to absorption and scattering per unit distance.

The amount of attenuation due to absorption is defined by the following relation⁷⁴

$$Q_a = \frac{-8\pi r}{\lambda} I_m \left\{ \frac{m^2 - 1}{m^2 + 2} \right\} \tag{5}$$

where I_m is the imaginary portion of the complex refractive index m . As shown in equations (4) and (5), wavelength plays a major role in defining the amount of attenuation due to scattering and absorption. With a wavelength of 10.6 μm, CO₂ lasers often experience greater plasma absorption^{74,77,78,83} than Nd:YAG lasers, which have a wavelength of 1.06 μm. At this lower wavelength, attenuation occurs primarily through scattering.^{74,76,78,84}

Forces affecting weld pool fluid flow

Heat transfer and fluid flow affect the size and shape of the weld pool, cooling rate and kinetics of various solid state transformation reactions in the fusion and heat affected zones (HAZs).^{24,58,70} Since heat transfer affects the thermal cycles, the structure and properties of the weldment are affected by the transport processes. There are several forces driving the circulation of liquid metal in the molten weld pool, including the surface tension, electromagnetic (in the case of arc or hybrid welding), buoyancy, and gas impingement or friction forces.

The main driving force affecting fluid flow in the weld pool is the Marangoni force, which arises from the spatial gradient of surface tension driven by the temperature and compositional gradients existing in the weld pool. The Marangoni stress τ is defined by⁸⁵

$$\tau = \frac{d\gamma}{dT} \frac{dT}{dy} + \frac{d\gamma}{dC} \frac{dC}{dy} \tag{6}$$

where $d\gamma/dT$ is the temperature coefficient of surface tension, dT/dy is the spatial temperature gradient on the weld pool surface and C is the concentration of surface

active elements. Of the two components in equation (6), temperature has a much greater impact on the magnitude of the Marangoni stress than the concentration of surface active elements.⁶⁶ The presence of surface active elements such as sulphur and oxygen in the steel weld pool has an impact on the direction of convection.^{85,86} If surface active elements are not present in the weld pool, the $d\gamma/dT$ term is negative, and liquid metal flows outwards from the heat source along the surface of the weld pool.⁸⁶ This flow causes the weld pool to become shallower and wider. If surface active elements are present in the weld pool, the $d\gamma/dT$ term is often positive,^{85,86} resulting in a reversal in the direction of liquid metal flow, with the liquid metal flowing inward from the solid/liquid boundary towards the heat source, leading to a deeper and narrower weld pool.⁸⁷

During arc welding, the interaction between the divergent current path in the weld pool and the magnetic field generated by the current flow produces the electromagnetic or Lorentz force.^{58,70} This force causes liquid metal to flow down along the centreline of the weld away from the heat source, tending to make the weld pool deeper.⁸⁷ The Lorentz force is defined by the following relationship⁸⁸

$$\mathbf{F}_{\text{emf}} = \mathbf{J}_c \times \mathbf{B} \quad (7)$$

where \mathbf{J}_c is the current density and \mathbf{B} is the magnetic flux in the weld pool.

The buoyancy or gravitational force arises from the spatial variation of the liquid metal density owing to temperature variations in the weld pool⁸⁹

$$F_b = \rho_l g \beta (T - T_{\text{ref}}) \quad (8)$$

where ρ_l is the density of the liquid metal, g is the acceleration due to gravity, β is the thermal expansion coefficient, T is the temperature of the liquid metal and T_{ref} is an arbitrary selected reference temperature. The magnitude of the buoyancy force is commonly very small and can be neglected.

During high current arc welding, the arc plasma can exert a frictional shear stress along the weld pool surface.⁹⁰ This frictional force causes liquid metal to flow from the middle of the weld pool towards the weld pool solid/liquid boundary.⁸⁷ The metal then circulates down along the solid/liquid boundary and up towards the heat source along the weld centreline resulting in a shallow and wide weld pool. For most welding conditions, this force is small and can be ignored, particularly at low and moderate currents.

The relative intensities of these forces dictate the convective heat transfer and the resulting weld pool geometry. There are several dimensionless numbers that are used to gauge the relative importance and order of magnitude of the forces affecting fluid flow and significance of convective heat transfer in the weld pool. These dimensionless numbers include the surface tension Reynolds number Re_s , magnetic Reynolds number Re_m and Peclet number which are defined in the equations below^{66,91,92}

$$Re_s = \frac{\text{Marangoni force}}{\text{viscous force}} = \frac{\rho_l L_R \Delta T |\partial\gamma/\partial T|}{\mu^2} \quad (9)$$

$$Re_m = \frac{\text{electromagnetic force}}{\text{viscous force}} = \frac{\rho_l \mu_m I^2}{4\pi^2 \mu^2} \quad (10)$$

$$Pe = \frac{\text{convective heat transfer rate}}{\text{heat transfer due to conduction}} = \frac{UL}{\alpha} \quad (11)$$

where ρ_l is the density of the liquid, L_R is the characteristic length of the weld pool and is assumed to be approximately half of the weld pool width, ΔT is the difference between the weld pool peak temperature and the solidus temperature of the material, $\partial\gamma/\partial T$ is the temperature coefficient of surface tension, μ is the liquid viscosity, μ_m is the magnetic permeability, I is the arc current, U is the characteristic velocity of the liquid metal, L is a characteristic length (half of the weld pool width) and $\alpha (=k/\rho C_p)$ is the thermal diffusivity of the material. The relative importance of the electromagnetic to Marangoni forces can be obtained from the ratio Re_m/Re_s . Under most arc welding conditions, the order of magnitude for the electromagnetic and Marangoni forces is the same. In laser welding, no electromagnetic force is present, and the Marangoni force is the primary cause of convection in the weld pool.

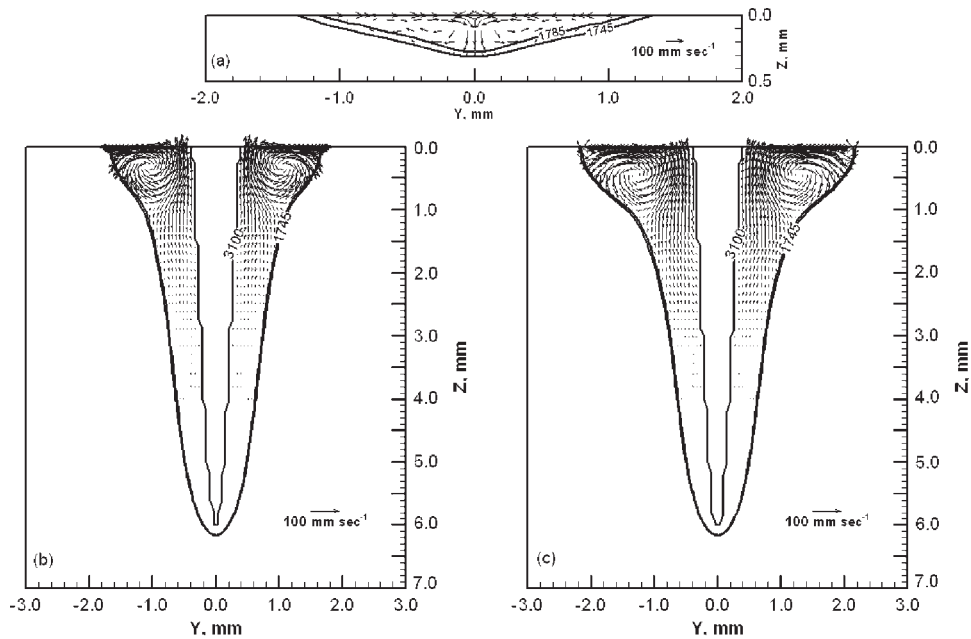
During welding, the rates of transport of heat, mass and momentum are often enhanced because of the presence of fluctuating velocities in the weld pool.^{19,66} The contribution of the fluctuating velocities is quantitatively expressed by an appropriate turbulence model^{66,93,94} that provides a framework for calculating effective viscosity and thermal conductivity values. The values of these properties vary with location in the weld pool and depend upon the local characteristics of fluid flow. The values of these properties vary with location in the weld pool and depend on the local characteristics of fluid flow.^{159,160} The specific model that is selected for these calculations depends on the level of rigor demanded by the application.⁹³⁻⁹⁵

Figure 4 shows the temperature and liquid metal velocity profiles for typical arc (Fig. 4a), laser (Fig. 4b) and hybrid welds (Fig. 4c). During arc welding, the fluid flow is mainly driven by the Marangoni and electromagnetic forces. The Marangoni force drives liquid metal from the middle of the top surface toward the edge of the weld pool and this force tends to widen the weld pool.⁸⁷ The electromagnetic force, on the other hand, tends to drive the liquid metal downward but it is often not as powerful as the Marangoni force. As a result, the shape of the weld pool during arc welding is often hemispherical. Similar fluid flow behaviour is seen in the case of conduction mode laser welding, where the weld pool shape is dictated by the Marangoni force and is hemispherical.

The depth of the weld pool during keyhole mode laser welding is influenced primarily by the presence of the keyhole.⁶⁵⁻⁶⁷ Marangoni convection moves the liquid metal on the surface of the weld pool towards the edge of the weld pool causing the upper part of the weld pool to be wider⁸⁷ than that of the lower portion shown in Fig. 4b. When both the arc and the laser is applied simultaneously in hybrid welding, both the electromagnetic and the Marangoni forces act to provide the flow pattern as shown in Fig. 4c. Here the depth is determined mainly by the keyhole,^{19,96,97} and the flaring of the weld pool at the top surface is determined mainly by the Marangoni force

Laser-material interactions

Laser welding can operate in either a conduction or keyhole mode.⁹⁸ The welding mode is dependent upon



4 Calculated cross-sectional temperature and fluid flow profiles for *a* arc, *b* laser and *c* hybrid welded A131 structural steel. The temperature isotherms are in units of Kelvin. The arc current and voltage were 191 A and 11 V. The laser power was 4.5 kW. The hybrid weld laser power was 4.5 kW and arc voltage and current were 12.3 V and 190 A respectively. All of the welds were performed at a welding speed of 0.51 m min^{-1} . The structural steel had an assumed sulphur content of $\sim 0.05 \text{ wt-\%}$

the power density of the heat source, physical properties of the material and welding speed.^{58,63,75,82} The hemispherical transverse weld cross-section obtained during conduction mode laser welding is similar to that obtained during arc welding.^{58,98} During conduction mode laser welding, the power density of the laser beam⁷¹ is typically less than 10^5 W cm^{-2} , leading to a shallower and wider weld pool than obtained during keyhole mode laser welding.^{58,71,98}

For keyhole mode laser welding, the power density of the heat source is greater than that typically used in conduction mode laser welding.^{58,98} Significant vaporisation of the workpiece surface also occurs, causing a vapour filled depression called a 'keyhole' to form in the laser generated weld pool.^{58,63,75,98} The geometry of the keyhole strongly depends on the power density distribution of the laser beam, the focal point of the laser, the composition and flow rate of the shielding gas, the welding speed and workpiece material.^{9,29,33,99}

The profile of the keyhole is often calculated by an energy balance at the keyhole wall, where temperatures are commonly assumed to be equal to the boiling point of the alloy.¹⁰⁰ The boiling point is the temperature where the sum of the vapour pressures of all alloying elements equals local pressure. The keyhole remains open due to the balance of surface tension, hydrostatic, vapour pressure, pressure gradient due to metal vapour flow and recoil pressures.^{63,100–102} The surface tension and hydrostatic pressures tend to close the keyhole, while the vapour pressure, pressure gradient and recoil pressure tend to maintain the keyhole. The balance of the keyhole pressures is given by^{63,100,102}

$$P_r + P_v + \Delta P = P_\gamma + \rho_l g h \quad (12)$$

where P_r is the recoil pressure, P_v is the vapour pressure, ΔP is the pressure gradient driving the vapour flow out of the keyhole, P_γ is the pressure due to surface tension

effects, ρ_l is the density of the liquid metal, g is the gravitational acceleration and h is the depth of the keyhole.⁶³ The recoil pressure term is defined by

$$P_r = J^2 / \rho_v \quad (13)$$

where J is the vaporisation flux calculated from the modified Langmuir equation^{66,103} at local temperatures along the keyhole surface, and ρ_v is the density of the evaporating gas particles. The pressure gradient due to vapour flow in the keyhole can be approximated as the cylindrical pipe flow pressure gradient based upon the Hagen–Poiseuille equation¹⁰⁴

$$\Delta P = 8\mu_v v_v h / r_k^2 \quad (14)$$

where μ_v is the viscosity of the metal vapour in the keyhole, v_v is the velocity of the metal vapour exiting the keyhole, h is the depth of the keyhole and r_k is approximated as the radius of the keyhole at half the depth. The metal vapour velocity is approximated by

$$v_v = J / c \quad (15)$$

where J is the vapour flux calculated from the modified Langmuir equation and c is the molar concentration of metal vapour in the keyhole. The surface tension pressure is given by⁶³

$$P_\gamma = a\gamma / r_k \quad (16)$$

where γ is the surface tension and the coefficient a has a value of 2 when close to the bottom of the keyhole in partial penetration welds. This value becomes 1 at other locations.

It is important to realise that the keyhole is constantly fluctuating.¹⁰⁵ Several studies have evaluated keyhole formation and proposed various mechanisms for describing keyhole instability.^{100,105–107} Keyhole stability is dependant in part on the power density of the heat

source, welding speed and workpiece material properties.¹⁰⁰ In the case of CO₂ lasers, the slope of the keyhole front wall affects the stability of the bottom of the keyhole.¹⁰⁶ The interaction of various forces can cause the keyhole walls to oscillate and collapse which can lead to porosity formation. Welding parameters such as laser focal position, welding speed and laser power can affect the ablation pressure and lead to fluctuations and keyhole collapse.¹⁰⁵

Physical processes driving arc–material interactions in GTAW and GMAW

The arc is a column of electrons and ions which flow between the anode and cathode of the welding circuit^{1,62,63,108} along the route of the lowest electrical resistance between the electrode and the workpiece.^{1,62,63,109} The arc column is often shielded by a layer of inert gas, which prevents oxidation and the entrapment of soluble gases in the liquid metal being welded. In addition, the shielding gas and surrounding atmosphere acts as a source of diatomic molecules for dissociation and ionisation during plasma formation. The plasma phase is a major factor affecting arc stability, especially since it comprises the majority of the arc column and contains the necessary ions and electrons for the energy transfer to the workpiece. Using a shielding gas with a relatively low ionisation potential decreases the resistivity of the arc column and increases arc stability. Introducing metal vapours into the arc plasma can also further reduce arc resistivity and enhance arc stability.^{1,110–112}

Important process parameters affecting GTAW include welding speed, arc length, arc current and the electrode polarity. These parameters affect weld pool fluid flow, thermal cycles and cooling rates, which can affect weld pool geometry, microstructure and mechanical properties. For arc welding performed at a constant current and velocity, arc radius decreases with decreasing arc length.¹¹³ As a result, the power density of the arc increases because the arc interacts with a smaller area of material.

In GMAW, liquid metal from a consumable electrode is added to the weld pool, increasing the process complexity by affecting the weld metal composition, heat input per unit length, weld pool cooling rate and fluid flow. The metal transfer mode affects the fluid flow, heat input per unit length and resulting quality of GMA welds,^{2,114} and is defined by the droplet shape and size, frequency and the mechanism by which droplets detach from the consumable electrode.

Three prominent modes of metal transfer are globular, short circuit and spray.⁶² During globular transfer, spherical droplets of molten metal build up at the electrode tip and detach at a relatively low frequency once they reach a size close to the diameter of the electrode due to the force of gravity.⁶² Globular transfer mode is often considered as the most undesirable of the three due to its high heat input, poor surface finish and the appearance of spatter in the final weld.^{2,114} Short circuit GMAW is characterised by molten metal bridging the gap between the electrode and weld pool causing a short circuit.¹¹⁴ Compared to globular transfer, short circuit mode GMAW results in a relatively higher quality surface finish with less spatter and has a lower heat input. Finally, in the spray transfer

mode, molten metal droplets with a diameter smaller than that of the electrode, are rapidly detached from the electrode tip by electromagnetic forces.^{62,114} Spray transfer mode requires relatively high voltages and has a high amount of heat input.¹¹⁴ Owing to the stable nature of the spray transfer mode, spatter is reduced and surface finish is improved.

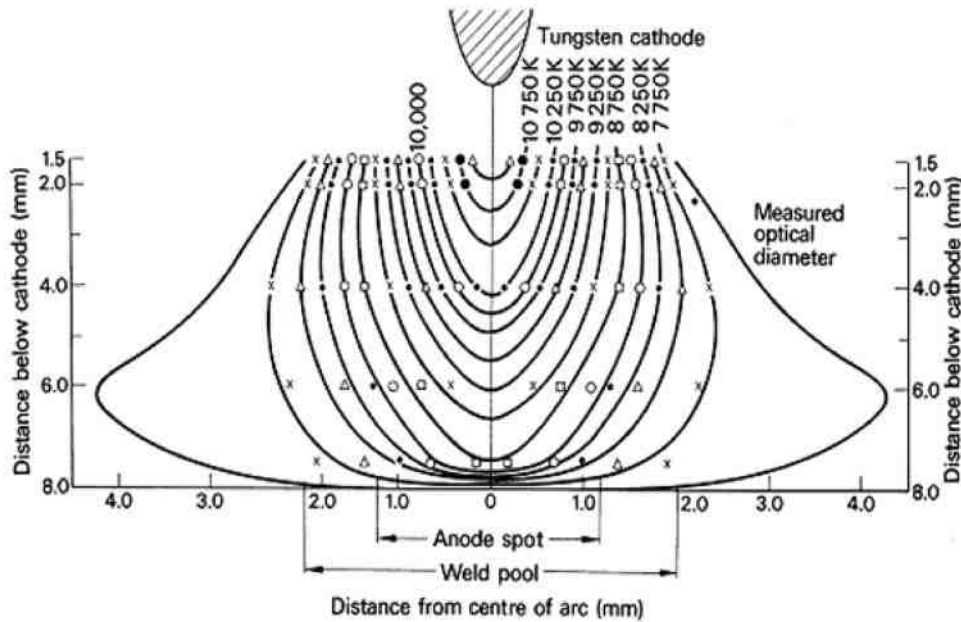
Characteristics of arc and laser plasmas

During arc and laser welding, a plasma phase is formed above the weld pool through the interaction between the arc or laser and the shielding gas. The plasma phase contains electrons, ions, excited atoms and molecules. Many of these species, particularly the excited atomic and molecular species, are not normally observed in gas–metal systems typically encountered in traditional materials processing.^{115–117} These excited species can significantly enhance the kinetics of reactions between the plasma phase and the material substrate. Knowledge of the number densities of these excited species and electrons can also provide insight into the important properties of the plasma and any dominant reaction processes. The electron temperature, which is a measure of the energy of the electrons within the plasma phase, is also an important parameter used to characterise the plasma phase. Because the laser and arc plasmas are formed at atmospheric pressures, the high collision rates result in the electron and heavy particle temperatures being nearly equal.¹¹⁸

Complex characterisation techniques, such as high temperature Langmuir probes or emission spectroscopy, are utilised to measure the electron temperature and species densities at discrete locations within the plasma phase.^{119–121} A Langmuir probe is a device which consists of one or more electrodes which are placed in a plasma phase with a constant or time varying electrical potential between the electrodes. The current and potential drops across the probes are then measured and correlated with the electron temperature and density of the plasma. Emission spectroscopy is a non-contact means for characterising the species present in the plasma phase. With this technique, species within the plasma phase are identified by their characteristic wavelengths. The intensities of the individual peaks can then be used to determine the species densities and temperatures within the plasma phase.

There are a number of differences between the properties of the plasma phases formed during arc and laser welding. The differences in the electron temperature and species density distributions present are primarily related to characteristics of the arc and laser heat sources and their interactions with both the shielding gas and the weld pool.^{122,123} For example, during laser welding, the vaporisation of alloying elements is relatively more pronounced because of the higher weld pool temperatures and the properties of the plasma are significantly affected by the metal vapours.^{103,124,125}

A number of researchers have investigated the characteristics of the plasma phase formed in the arc column during GTAW.^{122,126–128} Theoretical studies of the number densities of various species in a plasma phase have been performed. For example, Dunn and Eagar¹¹⁰ calculated the electron densities and the resulting transport properties of argon and helium



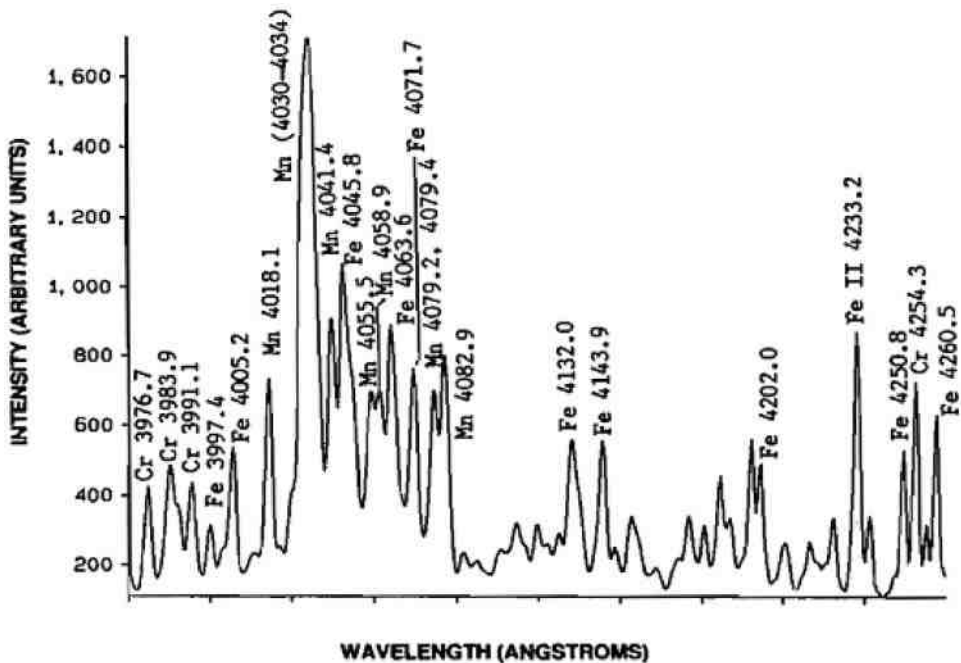
5 Temperature distribution in the arc column under GTAW conditions for an arc current of 100 A. The temperatures in the arc column were calculated using electrostatic probes¹²⁷

plasmas with small additions of metal vapours. Drellishak *et al.*^{129,130} investigated the species densities of both inert gaseous and pure nitrogen and oxygen plasmas at atmospheric pressures.

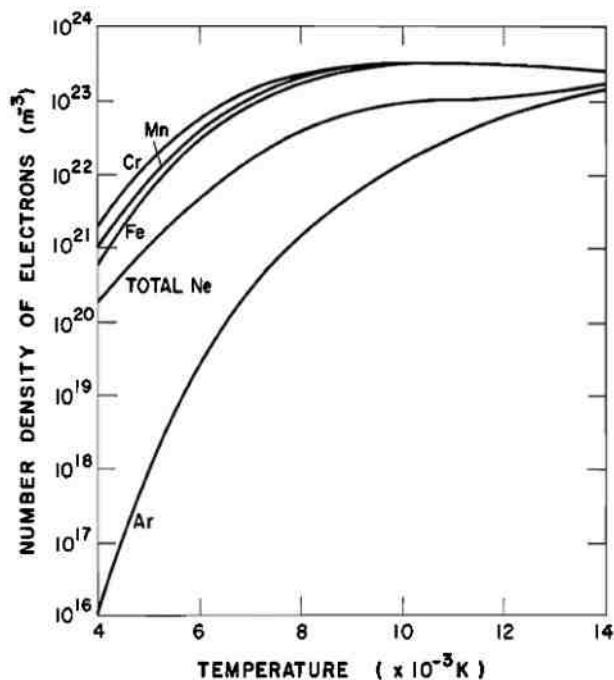
An example of temperature measurements made using Langmuir probes¹²⁷ in a GTAW arc is shown in Fig. 5. Temperatures at locations directly adjacent to the electrode are about 10 750 K. At these temperatures, ionisation of the gaseous species is prevalent. Throughout the remainder of the plasma phase in the arc column, the temperatures are high enough for significant dissociation of diatomic gases to occur and decrease as the workpiece is approached. Therefore, ionised species tend to dominate at locations closer to the electrode, and neutral species are dominant as the

workpiece is approached. Figure 5 also shows that the size of the arc plasma can have diameters of the order of 8 mm, which is considerably larger than the typical laser induced plasma.

During laser welding, the interaction between the laser beam and the alloy produces significant vaporisation of alloying elements, which vary depending on the composition of the alloy.^{103,124,125} For example, during laser welding of stainless steels, metal vapours may contain iron, chromium and manganese. Similarly, during laser welding of aluminium alloys, significant vaporisation of magnesium or zinc may take place.^{103,124,125} Figure 6 shows¹³¹ a typical optical emission spectrum of the plasma produced during CO₂ laser welding of AISI 201 stainless steel using helium shielding gas.



6 A typical spectrum of the plasma produced during laser welding of AISI 201 stainless steel using helium shielding gas¹³¹



7 Electron density as a function of electron temperature for various pure species as well as for a plasma formed during laser welding of AISI 201 stainless steel in argon shielding gas¹³²

Peaks containing excited and ionized Fe, Cr and Mn species are observed because of their presence in the plasma. Since the metal vapours are easily ionisable compared to the argon or helium shielding gas, their presence significantly affects the electron density and electron temperature of the laser induced plasma.

In addition to the metallic species, the shielding gas will also contribute some electrons to the plasma. At any given electron temperature, the equilibrium electron densities for each pure species can be computed considering the equilibrium condition for the ionisation of that particular species. In Fig. 7, the computed electron densities of pure metal vapours, including Fe, Mn and Cr, are significantly higher than that for argon over a range of electron temperatures in a laser plasma.¹³² If the composition of the plasma is estimated from the evaporation rates of each species and the subsequent mixing of these species in the shielding gas, the overall electron density can also be calculated by adding the product of the mole fraction of each species and its electron density for pure species.

When the metal vapours infiltrate the arc region, they have a significant effect on the resulting arc properties. It will be shown subsequently that the overlapping of the laser induced plasma plume with the arc can significantly affect the arc electron density and its electrical conductivity. Consequently, such overlapping can result in the establishment of a preferred current path that is different from that in the absence of the laser beam.

Physical processes governing arc-laser hybrid processes

Although the advantages of the hybrid welding process over those obtained from either arc or laser welding are well established, the fundamental physical processes are less well understood. Much of the existing literature

detailing laser-arc hybrid welding is based on empirical studies related to the process capabilities. In the following sections, the physical processes of laser-arc hybrid welding are more closely examined. Particular attention is paid to four important areas, including laser-arc interactions, the role of filler metal additions, the role of fluid flow in determining the weld pool geometry and identifying the mechanisms responsible for suppressing defect formation in hybrid welding.

Laser-arc interactions

Effect of laser on arc stability

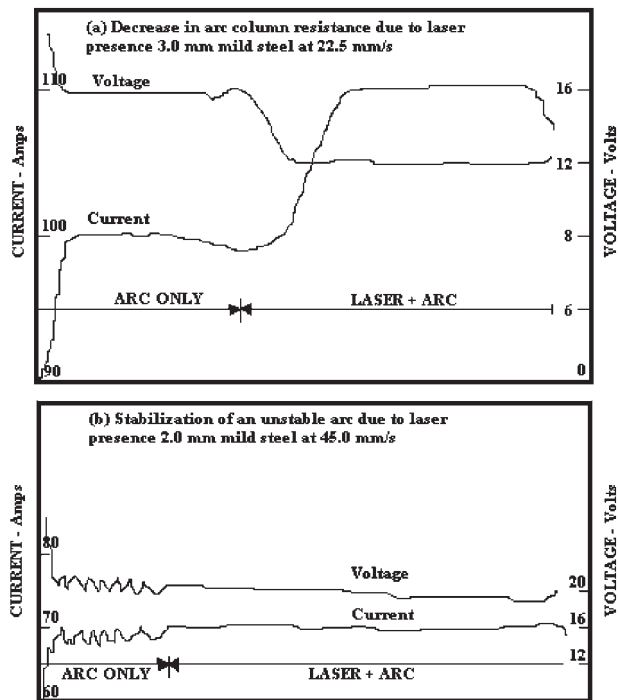
Since hybrid welding is often performed using a high power laser operating in the keyhole mode, the laser energy is absorbed through multiple reflections of the laser in the keyhole.^{58,84} A plasma phase is also formed by the interaction between the high power density of the laser heat source, the shielding gas and the metal vapour formed by the laser-material interaction. The plasma phase absorbs a portion of the laser energy,^{63,73,84,109} as described in detail in the section on 'Absorption of arc and laser'. Using a high ionisation potential shielding gas, such as helium, the formation of a laser induced plasma can be mitigated, particularly for high wavelength CO₂ lasers.^{9,14,29}

A plasma phase also forms by the interaction of the arc and the surrounding atmosphere during hybrid welding. The size of the arc plasma often depends on the distance between the heat sources and the arc current density, arc length and voltage. It has also been observed that the laser and arc plasmas interact, and the transmission of the laser through the plasma results in some additional laser attenuation.^{1,41,50,133} In the case of Nd:YAG laser/GTAW hybrid welding of mild steel,⁵⁰ the arc plasma absorbed up to 1% of the laser energy and the inverse Bremsstrahlung absorption coefficient was 0.01 cm⁻¹.

During hybrid welding, the arc undergoes a contraction in which its width is nearly the same size as the laser beam^{1,19,50,56} because the presence of the laser induced plasma causes the arc resistance and radius to decrease. Lower arc resistance and enhanced arc stabilisation¹ in the presence of a laser is shown via arc current and voltage data in Fig. 8. The influence of laser radiation on arc resistivity and stability can be explained by two phenomena. First, a small part of the laser energy is absorbed by the arc plasma, further ionising the arc plasma and reducing its electrical resistance.^{19,50,56,133} Second, significant vaporisation of the workpiece material occurs at the location where the laser impinges on the surface of the workpiece,^{58,131,132,134} and metal vapour is then transported into the arc plasma. Since the metal atoms have a much lower ionisation potential than the shielding gas, the effective ionisation potential of the plasma is reduced and a more conductive, stable plasma channel for the arc root and column is obtained.^{1,50,56,133} Since the arc follows the path of least electrical resistance, the arc tends to bend, and the arc root forms within close proximity to the keyhole.^{50,56,133}

Role of laser-arc separation

The roles that both heat sources play in these synergistic interactions are very significant. Often, hybrid welding is described as simply welding with an arc and a laser. However, changes in the distance between the arc and laser sources can cause two distinct welding processes,



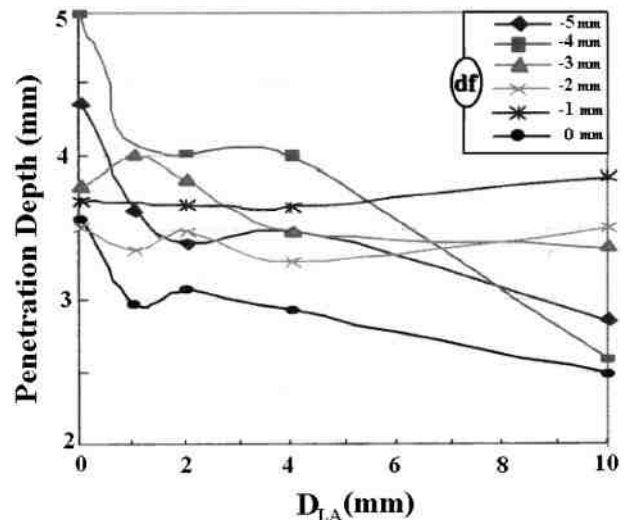
8 Characteristics of current and voltage during arc and hybrid welding: *a* arc resistance decreasing due to the presence of the laser; *b* laser stabilisation of fluctuations in arc voltage and current¹

hybrid and tandem welding, to emerge. During hybrid welding, an interaction occurs between the laser and arc plasmas as a result of the close proximity of the two heat sources. Tandem welding occurs when the distance between the heat sources is significantly greater than the arc plasma radius, usually 5–8 mm. In tandem welding, the arc and laser act separately on the workpiece.

The distance between the heat source focal points plays a large role in the arc and laser induced plasma interactions.^{1,42,50,133} Experimental research has shown that during the plasma interaction the contracted arc rooting in close proximity of the keyhole can increase weld pool penetration depth.^{42,50,56,133} This increase in depth is small relative to the penetration depth achieved by laser welding alone. In addition, the interaction results in a significant increase in weld pool width over laser welding.¹⁹ Beyond the fact that these weld pool dimensions increase due to the interaction of the plasmas, little scientific explanation as to the fundamental physical processes which occur to enhance these weld pool dimensions has been presented.

The effects of changes in arc current and voltage, welding speed, defocusing distance and laser to arc distance, and the effects on penetration depth, bead shape, spatter, arc stability and plasma formation were investigated during the CO₂ laser-GMAW hybrid welding of carbon steel.⁴² Figure 9 shows that as the distance between the heat sources decreases, the weld pool depth increases,⁴² which is in agreement with the findings of Naito *et al.*¹³⁵ In addition, an increase in negative beam defocusing may increase the penetration depth of the weld pool depending upon the operating mode of the laser beam and the depth of focus of the laser.

It has often been observed that the maximum penetration depth occurs at some intermediate distance

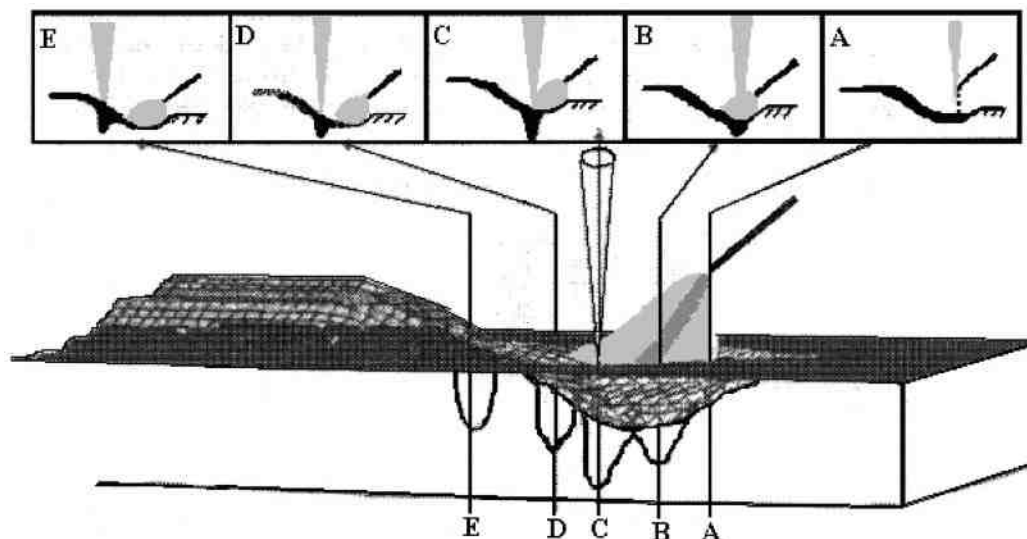


9 Effect of the distance between the arc root and laser focal point D_{LA} on weld pool penetration depth. In addition, the effect of defocusing (df) on penetration depth is shown⁴²

where the heat source interaction is optimised.^{2,42,56,135} Figure 10 is a schematic of how the hybrid welding penetration depth and weld pool geometry change for various separation distances between the heat sources.^{42,135} The maximum penetration depth was achieved when the laser passed through the edge of the arc plasma, versus through the centre or for a smaller separation distance. Very little is known as to why the penetration depth is not maximised when the separation between the heat sources is at its minimum, and a better understanding as to why this occurs would greatly benefit improving the reliability of the hybrid welding process.

The exact role of interheat source spacing on the interaction of the heat sources and its effects on the physical processes is not well defined and requires further research. When the distance between the laser and arc is significantly greater than the arc plasma radius, the laser and arc plasmas are separate. In contrast, when the distance between the two heat sources is less than or approximately the same as the arc plasma radius, the two plasmas interact.^{42,135} Therefore, the interaction of the laser beam and the arc plasma mainly depends on the distance between the heat sources, arc radius and arc plasma radius.^{1,41,50} A quantitative understanding of the interheat source spacing and its relationship with welding parameters will lead to a significant improvement in process control.

Recent research has examined the importance of the order in which the laser and arc are arranged during hybrid welding. For example, during hybrid welding of mild and stainless steels, the laser is placed in front of the arc in what is known as backhand welding.^{41,52} The main benefit of the arc following the laser is to decrease the high temperature gradient developed by the laser, resulting in decreased propensity for solidification cracking and increased toughness.³⁵ On the other hand, it is common during the welding of copper and other alloys with high reflectivity or thermal conductivity for the torch to be placed before the laser (forehand welding) in order to preheat the material before the laser passes.^{41,52}



10 Schematic of the effect of heat source separation distance on weld geometry and penetration. A, B, C, D and E indicate the change in relative position of the arc and laser in the weld pool (images above workpiece) and their corresponding weld bead geometry^{42,135}

The advantage of having the arc come before the laser is to increase both the amount of laser energy absorbed^{3,9,11,136} by the material and the efficiency of the laser energy input.^{41,50,133} However, experimental work performed on 304 stainless steel using Nd:YAG laser/GTAW hybrid welding has shown that the order of the heat sources has no clear effect on the depth of the weld.¹³⁵ A certain distance between the point of the arc and the laser beam needs to be maintained to ensure weld quality and that the interaction of the laser and arc plasmas is maintained.^{2,42,135} Naito *et al.*¹³⁵ showed that, when the arc is leading, hybrid welding does not always result in a greater weld pool depth, but the increase in depth is primarily dependent upon the distance between the heat sources. Further research is required on the role of heat source separation and its effect on plasma interactions, plasma formation and surface heating interactions of the heat sources.

Source of laser-arc synergy

The synergistic effect achieved in hybrid welding is illustrated by the surface heating interaction between the two heat sources, providing extra energy for welding with increased travel speed and enhanced penetration.^{9,133} The principle mechanisms of the synergistic interaction between the laser and arc in hybrid welding are commonly attributed to surface heating interactions, stabilisation of the arc cathode spot and constriction of the arc plasma column.^{1,50,56,133} Surface heating interactions are explained by the absorption of laser and arc energy by the workpiece and the nature of their power density distributions. Stabilisation of the arc cathode spot occurs through the introduction of metal vapours produced by the melting and intense vaporisation of the workpiece by the laser.^{112,131,134,137} A laser generated plasma has a higher electron density than other regions above the surface of the workpiece.^{1,131,132,138} Therefore, if the arc is close enough to the laser generated plasma, the plasma offers a line of least resistance or potential drop,^{1,50,139} coinciding with the Steenbeck effect, which states that the arc will always operate at the lowest possible potential.¹ Therefore, the arc root preferentially moves towards the laser generated hot spot.^{1,56,111} In

some cases, the arc has even been observed to bend in order to place the arc root at the laser generated hot spot.^{1,50,56,133}

The surface heating synergistic effect can be considered in terms of the heat transfer efficiency, which is defined as the fraction of heat provided by the heat sources versus the welding power, and the melting efficiency, which is the amount of energy provided by the heat sources which actually melts the workpiece. The heat transfer and melting efficiencies are given by¹³³

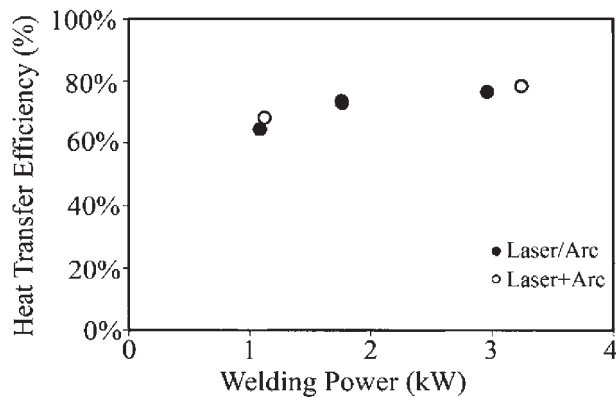
$$\eta_h = Q_i / Q_o \quad (17)$$

$$\eta_m = Q_m / Q_i = Av\rho \left(\int_{T_o}^{T_m} C_p dT + H_f \right) / Q_i \quad (18)$$

where η_h is the heat transfer efficiency, Q_i is the heat transfer rate, Q_o is the welding power, η_m is the melting efficiency, Q_m is the melting rate, A is the area of the transverse weld cross-section, v is the welding speed, ρ is the density of the material, C_p is the heat capacity of the material, T is temperature, T_o is the ambient temperature, T_m is the melting temperature of the material and H_f is the latent heat of fusion of the material.⁴¹

Figure 11 shows the heat transfer efficiency as a function of the welding power during tandem and hybrid welding.¹³³ Over the range of welding powers Q_o considered, the hybrid welding process does not have a synergistic advantage as far as heat transfer is concerned.¹³³ It is known that the heat transfer efficiency of the laser welding process is closely related to keyhole formation. Therefore, changing from conduction to keyhole mode laser welding increases the heat transfer efficiency due to multiple reflections of the incident radiation inside the keyhole.^{58,84,133} However, there is no change from conduction to keyhole mode laser welding depicted in Fig. 11.

It is important to establish whether the interaction between the heat sources is purely material or process parameter dependent. The interaction of the arc with the laser generated keyhole would affect keyhole dynamics,



11 Heat transfer efficiency as a function of welding power when the arc and laser are performing (laser+arc) tandem welding or (laser/arc) hybrid welding¹³³

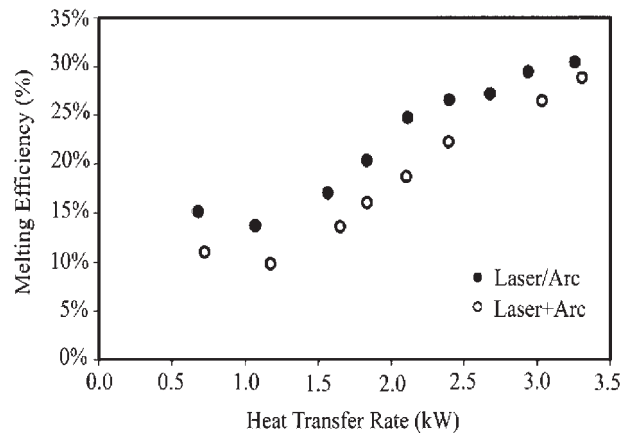
stability and fluid flow. Particularly, the arc rooting in the laser generated keyhole could account for an increase in keyhole fluid flow along the walls and around the keyhole, thus enhancing keyhole stability and slightly increasing the penetration depth.^{42,56,135} In addition, the arc rooting in the keyhole may affect the recoil and pressure gradient terms in the keyhole pressure balance and slightly enhance keyhole stability.

Figure 12 shows the melting efficiency as a function of the heat transfer rate for hybrid and tandem welding.¹³³ The melting efficiency of hybrid welding shows a significant improvement over that observed during tandem welding.^{9,140} However, the degree of interaction between the two heat sources is unclear.¹³³ The observed synergistic effect is explained by two phenomena.^{50,133} First, an increased stability of the arc cathode spot on the workpiece surface improves the melting process.^{50,133} Second, the arc is constricted by the laser, leading to a higher power density and more efficient melting,^{9,50,56,133} which is caused by increased ionisation due to the absorption of the laser by the arc plasma and the transport of vaporised metal from the keyhole into the arc plasma.^{9,50,56,133}

A clear distinction must be made as to when the arc and laser are acting in combination and when they are acting separately. This conclusion will aid in defining the hybrid welding process and help to develop a comprehensive understanding of the heat source interactions which occur during hybrid welding. Recent work has focused on the surface heating interaction of the heat sources and the interaction between the shielding gas and metal vapours ejected from the keyhole and the arc plasma,^{9,11} which can affect keyhole dynamics, heat transfer and fluid flow, weld pool geometry, cooling rates, and hence the structure and properties of the weld.

Role of filler metal additions

Laser/GMAW hybrid welding allows for the possibility of further modifying the weld bead shape, eliminating undercut, increasing gap bridgeability and reducing the propensity for cracking, and porosity through improved weld composition.^{2,12,22,38} These process improvements are due to filler metal additions provided by the GMAW process. With the inclusions of this process, the overall complexity of the hybrid process is increased by changes in the dominant metal transfer mode and weld metal composition.



12 Melting efficiency as a function of the heat transfer rate. The two datasets show the arc and laser during (laser+arc) tandem and (laser/arc) hybrid welding¹³³

The metal transfer mode affects the heat input and fluid flow of the weld pool due to droplet energy and momentum transfer. Depending upon the metal transfer mode, metal droplet size and droplet frequency, filler metal can increase the volume of the weld pool and the amount of heat input from the arc heat source.^{22,42,96,141} Spray transfer, because of its high heat input per unit length and ability to reduce spatter, is the most appropriate metal transfer mode for laser/GMAW hybrid welding.⁴² The result is a relatively larger weld bead with good surface finish. Short circuit transfer is not often preferred due to instabilities generated in the molten pool.^{2,42}

Filler metal additions have been observed to increase the stability of particular microstructural morphologies, such as acicular ferrite, or reduce the propensity for solidification cracking²² by modifying the weld pool composition. The extent of mixing of the filler metal plays an important role in determining weldment properties and is primarily affected by the rate of mixing (fluid flow) and cooling rate (solidification time) of the liquid metal.¹⁴² Zhou *et al.*^{141,142} have developed numerical models to evaluate the transport phenomena during laser/GMAW hybrid welding. They observed that the filler metal wire diameter and droplet size have a significant effect on the fluid flow in the molten weld pool. Increasing the droplet size, or filler metal wire radius, increases the impinging droplet momentum and the lateral diffusion of filler metal in the weld pool.¹⁴² In addition, adding larger droplets to the weld pool increases the heat input and can reduce the cooling rate of the weld pool.¹⁴²

Fluid flow and weld pool geometry

One of the most beneficial aspects of combining laser and arc sources in hybrid welding is improved weld geometry at high welding speeds.^{2,10,11,96} A quantitative understanding of the effects of the Marangoni, Lorentz, buoyancy and impingement forces is essential in furthering the understanding of hybrid welding. By understanding the quantitative role which these forces play in dictating weld pool temperature profiles, fluid flow, and geometry, the effects of hybrid welding on reducing the propensity for cracking, porosity and brittle phase formation can be further understood.

Little work, though, has been carried out to quantitatively understand the fluid flow within the molten weld pool during hybrid welding.^{19,141,142} The use of X-ray transmission imaging of Pt and W markers during hybrid welding shows that there is a strong liquid flow towards the rear of the weld pool.^{99,135} The fluid flow in the molten weld pool causes heat to flow away from the keyhole, thus elongating the weld pool.^{135,143} The flow is believed to be driven primarily by electromagnetic and surface tension forces.^{19,135}

According to the current process understanding, the primary process parameters which affect bead geometry in hybrid welding are laser power, arc power, welding speed, laser beam radius, defocusing and the distance between the heat source focal points.^{19,22,56,96} Weld pool depth is primarily affected by the laser power, power density and welding speed.^{19,96} Currently, it is believed that the arc power is the primary processing factor in establishing the width of the weld pool^{96,135} because the arc is a more dispersed heat source. During GTAW and GMAW, increasing arc current increases the arc radius, reduces arc penetration and increases the width of the weld pool. As the power density distribution of the arc heat source becomes more dispersed at high currents, the current density decreases, thus decreasing the Lorentz force.

Welding speed has a direct effect on the heat input per unit length per unit time of the welding process. At faster welding velocities, heat input decreases for a constant arc and laser power, since the heat source interacts with the workpiece for a shorter amount of time. Less molten metal is thus generated by the heat sources, causing both the width and penetration depth of the weld pool to decrease.

The laser beam radius at the workpiece surface can also be altered by defocusing the heat source. Negative defocusing of the laser may increase the penetration depth of the weld pool due to the convergent nature of the laser beam.^{42,60,98} As the convergent laser beam travels into the workpiece, the power density of the laser beam increases. Therefore, increasing the amount of negative defocusing can increase the keyhole depth and weld penetration. However, if the defocusing exceeds a critical value, keyhole formation will be inhibited and the weld penetration will decrease. In the case of positive defocusing, the keyhole depth decreases because the laser beam converges at a location above the workpiece surface, thus hindering keyhole formation and laser beam energy absorption.

The power level ratio between the laser and the arc also can play a significant role in the hybrid welding process. This ratio can be used to determine whether the laser or the arc is dominant and which one has the greater influence on the change in penetration depth and the width of the weld pool.^{96,133} El Rayes *et al.*⁹⁶ showed that increasing the ratio of arc to laser power, for constant CO₂ laser power levels of 8 and 4 kW, causes the narrow lower portion of the hybrid weld cross-section to increase in length. However, there appears to be minimal effect on the total depth of the weld pool.

The effect of the power ratio on laser vaporisation and laser attenuation by the arc plasma has been experimentally observed during CO₂ laser/GTAW hybrid welding.⁵⁶ When the arc current is greater than a critical level for a specified laser power, the interaction between

the laser induced and arc plasmas is less prominent.^{56,144} The result is reduced keyhole stability and a weld cross-section similar to a conduction mode laser weld.⁵⁶ The attenuation of the laser beam by the arc plasma keeps the laser from generating a significant amount of metal vapour necessary to continue the plasma interaction between the arc and laser.

Understanding the effects of power level ratio, heat source separation and laser defocusing on fluid flow and weld pool geometry is essential for more complete understanding of hybrid welding. The combinations of these important process parameters during the synergistic interaction between the arc and laser induced plasmas have not been thoroughly discussed in the literature. A fundamental understanding of the roles which these processing parameters play during hybrid welding, particularly when an arc-laser plasma interaction is occurring, would greatly benefit the welding industry to improve process control.

Defect formation

Hybrid welds contain much lower levels of porosity in both size and number than laser welds.^{26,27,135,145} The reduced presence of porosity in hybrid welds has been largely attributed to the lower cooling rate of the liquid weld pool compared to laser welding. The addition of the arc heat source reduces the solidification rate and allows for gas porosity to leave the molten metal. However, much further research is required in order to understand porosity formation, particularly in the case of porosity due to unstable keyhole collapse.

The formation of microporosity (<1 µm diameter) has been attributed to the entrapment of gases such as dissolved hydrogen or air. Larger macroporosity can also arise from the unstable collapse of the laser induced keyhole during laser or hybrid welding due to fluctuations of welding process parameters. For example, the focal point of the laser, laser power or welding speed. In addition, macroporosity has been attributed to the coalescence of microporosity in the case of laser beam welding of magnesium alloy AM60B.¹⁴⁶

Studies on the formation of macroporosity in magnesium AZ31B hybrid butt welded plates showed that the composition of the surface of the pores was 24.8 wt-% oxygen and 9.4 wt-% nitrogen.^{26,27} Air from the atmosphere can enter the weld and generate nitrides and oxides. The remedy to this problem is the addition of shielding gas for the laser.^{26,27} In the case of laser welding of magnesium alloy AM60B, the porosity was attributed to the evolution of hydrogen gas pores due to the difference in hydrogen solubility between the liquid and solid phases.¹⁴⁶ Subsequent welding passes lead to the coalescence of these pores and resulted in much larger macropores.¹⁴⁶

Blowhole macroporosity occurs during the laser lap welding of zinc coated steels.^{52,54,147} The boiling point of zinc is approximately 900°C, which is significantly lower than the melting point of iron (1538°C). When zinc coated sheets are lap welded, zinc vapour filled bubbles form and blowholes are generated in the final weldment.^{52,54,147} With laser/GMAW hybrid welding, the formation of blowholes and porosity are significantly diminished as compared to laser welding because a much longer time elapses before the molten metal solidifies, allowing for the bubbles to escape.^{147,148}

Additional defects can be caused, particularly in laser welding, by gaps which may form due to improper joint fit-up. The ability to bridge larger gaps during hybrid welding means less edge preparation. Because of the restricted width of the laser beam, perpendicular workpiece edges are required in laser welding.⁴¹ The addition of liquid metal to the weld pool makes laser/GMAW hybrid welding a beneficial process for bridging gaps between workpieces.^{41,62,63,114} The wide power density distribution of the arc heat source allows for less stringent gap tolerances during hybrid welding than laser welding.^{7,41,145,149}

Microstructure and properties

Understanding how the cooling rate changes with hybrid welding parameters can explain why the microstructure and mechanical properties of hybrid welds differ from those attained during arc or laser welding. In the following sections, the authors discuss the role of heat input and power density on microstructural formation and the effects of hybrid welding, relative to laser or arc welding, on weldment microstructure and mechanical properties for steels, magnesium and aluminium alloys.

Role of heat input and power density

Weldment cooling rate is dependent upon the thermo-physical properties of the material, power density (W mm^{-2}) of the heat source^{21,62,63,150} and heat input per unit length of the welding process (J mm^{-1}).^{4,6,20,151} The heat input per unit length is dictated by the welding speed and power of the heat source and given by²⁰

$$H = \frac{P_n}{v} \quad (19)$$

where H is the heat input per unit length in J mm^{-1} , P_n is the nominal power of the heat source in W and v is the welding speed in mm s^{-1} . Decreasing the heat input per unit length of the welding process results in more rapid heating and cooling rates.^{12,20,63} The cooling rate has a major effect on the microstructure of welds and this topic is discussed in the next section. In addition, welding processes with lower heat input per unit length result in a relatively lower amount of grain coarsening^{20,21,62,152} which gives the welded material higher strength. For example, GTAW of Ti-6Al-4V⁶¹ showed that the average prior β grain size decreased from approximately 360 to 60 μm upon decreasing the heat input from 4330 to 2130 J mm^{-1} . In the case of GMAW of HSLA-100 steel, decreasing the heat input from 4000 to 1000 J mm^{-1} resulted in a decrease in the HAZ prior austenite average grain size from 130 to 80 μm .¹⁵³

Even though the hybrid welding process results in a higher heat input per unit length than laser welding, it still retains high productivity and deep weld penetration.^{12,20,154} Hybrid welding is performed at welding velocities similar to laser welding, but the additional energy input by the arc increases the heat input per unit length.^{20,21} For example, a hybrid weld made at 1 m min^{-1} with a 2.8 kW laser and a 191 A, 14 V arc results in a heat input per unit length of 489 J mm^{-1} . Therefore, hybrid welding allows for the weld metal to remain at high temperatures for longer times and cool at lower rates compared to a 2.8 kW laser weld performed at the same welding speed.^{20,21} The result is a coarser

microstructure with a reduced percentage of brittle phases and increased toughness and lower hardness.

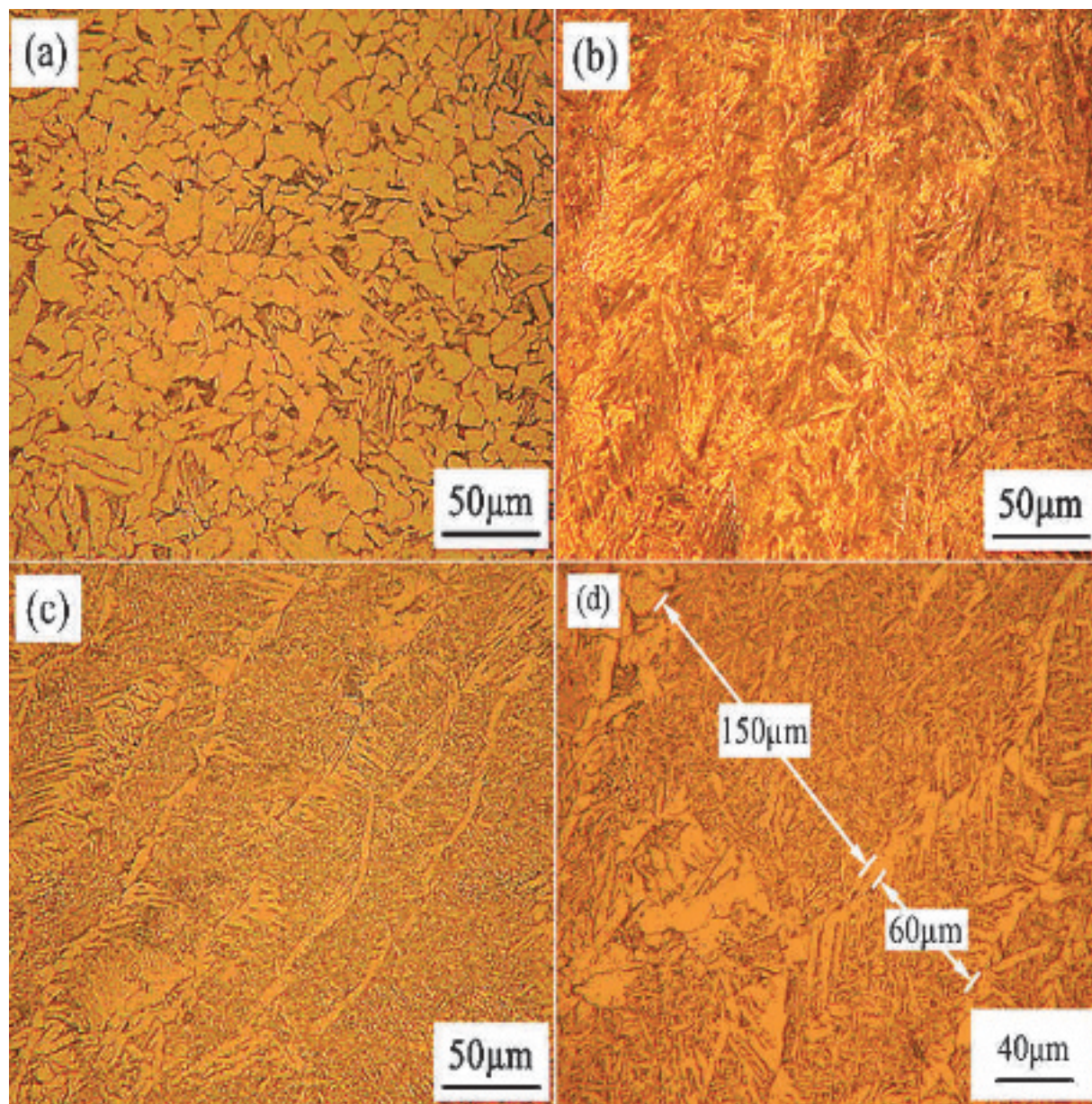
Weld microstructures vary as a function of the distance relative to the weld pool centreline. Differences in the peak temperature experienced by the material, the cooling rate and composition at different locations lead to the formation of three regions of varying microstructures. The regions in order of increasing distance from the weld centreline are the fusion zone, HAZ and base metal.^{20,58,62} By adjusting heat source power density, heat input per unit length and filler metal additions the microconstituents, mean grain size, and width and shape of the HAZ and fusion zones can be modified, thus ultimately affecting the mechanical properties of the weldment.^{12,20,62,154}

Steel hybrid welds

Steel microstructures can be manipulated by controlling the cooling rate and weld metal composition. During autogenous laser welding, no filler metal additions are made, which significantly limits the range of alloys that can be laser welded. For many important high strength steels, filler metal additions are required in order to avoid solidification cracking and the formation of brittle phases. The ability of the hybrid welding process to incorporate filler metal additions provides it with a marked advantage over autogenous laser welding and allows a much larger range of steels to be welded in a single pass at high travel speeds.

The application of hybrid laser/GMAW welding has been limited primarily to the welding of low carbon steels.²⁰⁻²² These studies have focused on the microstructures formed during the hybrid welding process and have examined the role of filler metal additions.²⁰⁻²² During the welding of pipeline steels, metal cored wire filler metal additions promote the nucleation of ductile acicular ferrite, which improves the material toughness compared to autogenous laser welding.²² Comparison of the weld pool cooling rates for laser and hybrid welding showed that the time to cool from 800 to 500°C was 2.9 s for hybrid welding and 2.2 s for the laser welding for the conditions of welding investigated.²² The laser microstructures were relatively fine and consisted of acicular ferrite, Widmanstätten ferrite and bainite, while the hybrid structures consisted of coarser acicular ferrite and Widmanstätten ferrite.²²

Recent research has also focused on the role of heat input on changes in the weldment microstructure for laser, GMA and laser/GMAW hybrid welding.²⁰⁻²² Figure 13 shows micrographs of the base metal (Fig. 13a), laser (Fig. 13b), arc (Fig. 13c) and hybrid (Fig. 13d) weld microstructures.²¹ The mild steel base metal has a mean grain size of 25 μm and equiaxed ferrite with sparse amounts of pearlite.²¹ After laser welding at a heat input of 338 J mm^{-1} , the microstructure consisted primarily of lath martensite in the weld fusion zone with a small fraction of proeutectoid ferrite at the prior austenite grain boundaries.²¹ The width of the laser weld HAZ was relatively small compared to hybrid or arc welding due to the lower heat input per unit length.^{20,21} Arc welding (432 J mm^{-1}) resulted in a coarser fusion zone microstructure and wider HAZ than that of the laser or hybrid welds due to the low power density and high heat input of the arc welding process.²¹ The arc weld fusion zone²¹ microstructure was composed of columnar proeutectoid



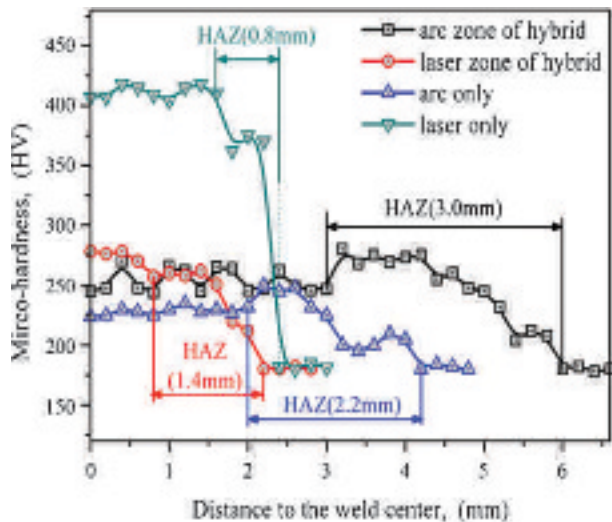
13 Micrographs of mild steel *a* base metal, *b* laser, *c* arc and *d* hybrid weld microstructures.²¹ The laser and hybrid weld laser power was 4.5 kW. The GTA and hybrid welds' arc current was 180 A. The welding speed for all welds was 13.33 mm s⁻¹

ferrite with intergranular acicular ferrite and pearlite. The hybrid weld (770 J mm^{-1}) displayed a higher heat input than the arc weld, resulting in a fusion zone microstructure that contains a larger amount of pearlite than the arc weld.²¹

Microhardness profiles are shown in Fig. 14 for the arc, laser and hybrid welding of mild steel.²¹ The fusion zone of the laser weld has the highest microhardness of the three welding processes and is significantly higher than that of the base metal, due to its small grain size and large fraction of martensite. The hardness and strength values of the arc fusion zone are lower than those for laser and hybrid welds due to a coarser grain size and the presence of ferrite and pearlite. Compared to laser welding, the additional heat input from the arc during hybrid welding reduces the cooling rate of the weld and prevents the formation of martensite. The relatively higher amount of pearlite present in the hybrid

weld fusion zone, compared to arc welding, contributes to its higher strength and hardness.

The current literature indicates that the hybrid welding process improves the weld metal microstructure.^{30,41,155,156} However, changing the heat input per unit length can cause the hybrid welding process to produce microstructures similar to laser or arc welding.²⁰ Relatively high heat input laser/GMAW hybrid welding of medium carbon steel resulted in the formation of coarse columnar grains in the weld fusion zone.²⁰ At a heat input of 796 J mm^{-1} using an arc current and voltage of 120 A and 28 V and laser power of 5 kW, and at a travel speed of 540 mm min^{-1} , the columnar grains were composed of proeutectoid and acicular ferrite, and the microstructure contained intergranular pearlite.²⁰ The HAZ of these welds were composed of a large fraction of coarse pearlite with intergranular proeutectoid ferrite.



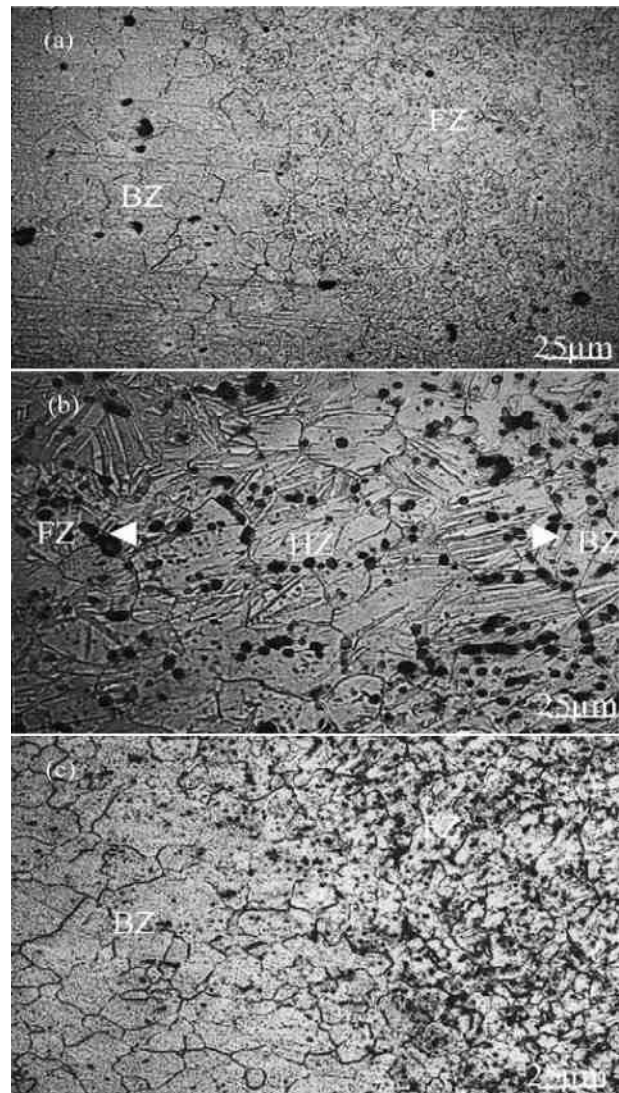
14 Microhardness as a function of distance from the weld centreline for arc, laser and hybrid welds made on mild steel samples. The hybrid weld is represented by two microhardness profiles. The arc zone is located closer to the surface of the weld pool, while the laser zone of the hybrid weld is located closer to the weld root. The arc and laser weld microhardness samples were taken relatively close to the weld pool surface²¹

Decreasing the heat input per unit length (547 J mm^{-1}) results in the formation of a much finer microstructure composed of very little proeutectoid ferrite and the weld fusion zone is primarily martensite.²⁰ The HAZ is primarily composed of martensite with intergranular proeutectoid ferrite.²⁰ The drastic change in the microconstituents of the medium carbon steel is due to the large differences in the heat input and cooling rate. The temperature gradients and cooling rates in the low heat input hybrid weld are greater than the higher heat input case.

Magnesium and aluminium hybrid welds

Magnesium alloys can be easily recycled and have a relatively high strength to weight ratio, making them an attractive alternative to replace denser structural materials. One of their primary disadvantages lies in the difficulty typically encountered when welding them using conventional processes. Since magnesium alloys are precipitation hardened, the heat input per unit length of the welding process becomes very important, particularly in terms of its effect on precipitate size, shape, and distribution and grain size and orientation of the α phase, making them good candidates for hybrid welding.¹⁵² Research on the hybrid welding of magnesium alloys (primarily AZ31B) has focused on the laser/GTAW process.^{6,55,152,155}

The microstructure of AZ31B magnesium alloys is composed of equiaxed α -Mg (HCP) with interspersed ellipsoidal β - $\text{Mg}_{17}(\text{Al,Zn})_{12}$ precipitates.^{152,157} Nd:YAG laser welding of 1.7 mm thick AZ31B magnesium alloy using a 400 W laser shown in Fig. 15a results in fine equiaxed grains and precipitate coarsening in the weld fusion zone.⁶ Although the microstructure is fairly homogeneous in the AZ31B magnesium laser weld fusion zone, the grain size is smaller than that of the base metal. The mean grain size for the base metal α



15 Fusion zone (FZ), heat affected zone (HZ) and base metal (BZ) microstructures for a laser, b GTA and c hybrid welded AZ31B magnesium alloy.⁶ The laser power was 400 W for the laser and hybrid welds. The arc current for the arc and hybrid welds is approximately 70 A

phase is approximately $25 \mu\text{m}$, and base metal β precipitates are on the order of 200 nm in length.¹⁵² The mean grain size of the laser weld fusion zone α phase is approximately $6 \mu\text{m}$, but the length of the β precipitates is not apparent.⁶ Coelho *et al.*¹⁵² evaluated laser, arc and hybrid welding of AZ31B magnesium alloy and determined that the lengths of β phase precipitates in the fusion zone after laser welding are between 300 and 500 nm .¹⁵² Precipitate coarsening likely results from segregation of alloying additions within the fusion zone.¹⁵²

Gas tungsten arc welding of 1.7 mm thick AZ31B magnesium alloy at 70 A results in a mean fusion zone grain size of $30 \mu\text{m}$, as shown in Fig. 15b.⁶ The fusion zone microstructure was composed of an α -Mg matrix with α -Mg + β - $\text{Mg}_{17}\text{Al}_{12}$ eutectic phase, which was much coarser in the fusion zone than HAZ.^{6,158} The HAZ microstructure is predominantly α -Mg with small β precipitates.^{6,158} In the case of GTA welding of AZ31B magnesium alloy, the HAZ width is much larger than

that obtained during laser welding, and the high heat input of the arc process results in significantly larger grains.¹⁵⁸

On the other hand, hybrid welding tends to result in a fusion zone weld microstructure composed of equiaxed α -Mg grains which are intermediate in size compared to that obtained through laser and arc welding. Fig. 15c shows the fusion zone and base metal microstructures of 400 W laser power, 70 A arc current hybrid welded AZ31B magnesium alloy.⁶ The β precipitates in the fusion zone are much coarser than that in the base metal.⁶ The quantitative effects of heat input on β precipitate sizes for GTAW and hybrid welding are unknown and would be a beneficial area of research in order to further the application of hybrid welding magnesium alloys.

Changes in weld microstructure influence the mechanical behaviour of the weld material relative to the base metal. Table 2 compares the microstructural features and mechanical properties of AZ31B arc, laser and hybrid welds. In the longitudinal direction, the laser fusion zone and base metal yield and ultimate tensile strengths are similar,¹⁵² but the ductility of the fusion zone is lower. In the case of arc welded AZ31B magnesium alloy, the tensile strength is approximately 94% that of the base metal.¹⁵⁸ The HAZ and fusion zone have similar microhardness values, which are slightly less than that of the base metal due to grain coarsening.¹⁵⁸ In the case of hybrid welding, the mean grain size is similar to that of the base metal, resulting in similar microhardness.⁵⁵ Currently, little mechanical testing has been performed on AZ31B magnesium alloy hybrid welds. Further testing of the tensile behaviour and

microstructural characterisation of hybrid welds compared to that of the base metal would highly benefit the further application of hybrid welding for magnesium alloys.

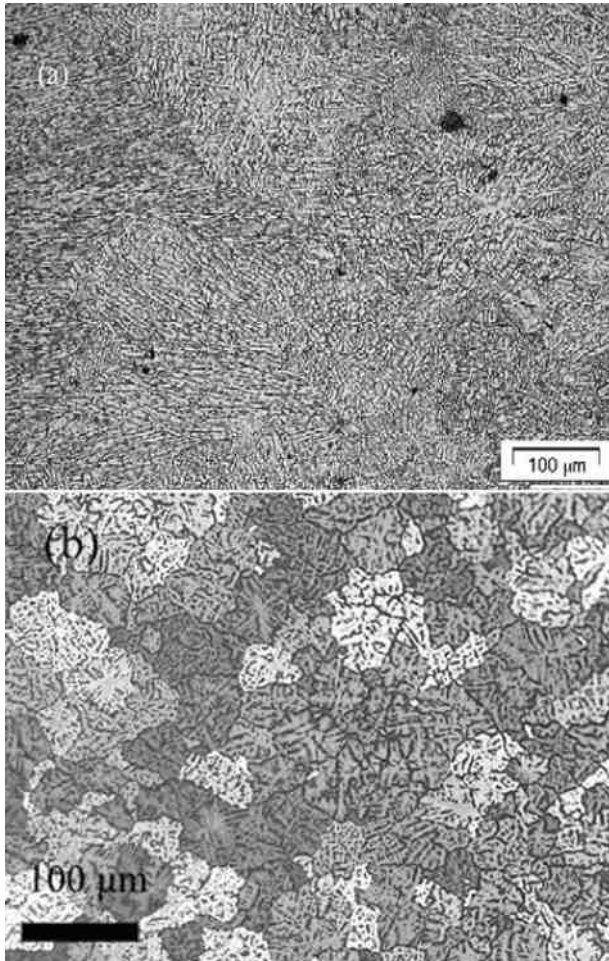
While the relatively high thermal conductivity and reflectivity to laser radiation^{4,24,150,151} can be overcome in the laser welding of Al alloys, the ability to easily add filler metals during hybrid welding makes it very attractive to join large sections of aluminium sheet quickly. Most of the current research on hybrid welding of 7xxx series aluminium alloys uses the laser/GMAW hybrid welding process.^{4,24,150,151} These aluminium alloys gain their strength via precipitation hardening.⁴ The size and distribution of these precipitates are dictated primarily by the temperature cycles and alloying element additions in the weld fusion zone.⁴

Hybrid⁴ and laser¹⁵¹ welding of 7xxx series aluminium alloys with the addition of filler metal result in very similar microconstituents,^{4,24,151} as shown in Fig. 16. However, the fusion zone mean grain size for hybrid welding is larger than that for laser welding. The microstructures consist of columnar dendrites at the fusion zone boundary and fine equiaxed grains along the weld centreline. During solidification, segregation of the alloying elements causes precipitates or eutectic films to form along the dendrite boundaries in the fusion zone,⁴ resulting in decreased ductility.⁴ The hybrid weld HAZ width is significantly larger than of the laser weld due to a relatively higher heat input. It is important to have a low heat input per unit length in order to retain more of the base metal mechanical properties.

Autogenous laser (Yb fibre laser and Nd:YAG) and laser/GMAW hybrid welding processes cannot achieve

Table 2 Microstructural features and mechanical properties of AZ31B magnesium alloy arc, laser and hybrid welds

	Base metal	Arc welding	Laser welding	Hybrid welding
Microstructure and grain size	Equiaxed α grains with mean ⁶ grain size of 25 μm β precipitates ¹⁵² with max length of 200 nm	30 μm mean grain size ⁶ Coarse α -Mg matrix with eutectic α -Mg + β -Mg ₁₇ Al ₁₂ eutectic phase ¹⁵²	Columnar α grains with mean ⁶ grain size of 6 μm Coarse β precipitates ¹⁵² with max length of 300–500 nm	Equiaxed α -Mg grains of varying size ⁶ Mean α grain ⁶ size of approximately 20 μm No quantitative data for precipitate sizes
HAZ microstructure, grain size and width		Predominantly α -Mg with small precipitates ¹⁵⁸ Grain size ¹⁵⁸ ranges from 10 to 60 μm HAZ width ¹⁵⁸ is approximately 0.3 mm	HAZ microstructure is similar to that of base metal with little β precipitate coarsening ¹⁵² HAZ width ¹⁵² is 10 μm	HAZ width is approximately 0.2 mm ⁵⁵
Ultimate tensile strength	249 \pm 5 MPa in longitudinal direction ¹⁵² 251 \pm 5 MPa in transverse direction ¹⁵²	Approximately 230 MPa ¹⁵⁸	247 \pm 5 MPa in longitudinal direction ¹⁵² 247 \pm 5 MPa in transverse direction ¹⁵²	
Yield strength	146 \pm 5 MPa in longitudinal ¹⁵² direction 148 \pm 5 MPa in transverse direction ¹⁵²		134 \pm 5 MPa in longitudinal ¹⁵² direction 92 \pm 5 MPa in transverse direction ¹⁵²	
Per cent elongation	20 \pm 1.5% in longitudinal ¹⁵² direction 24 \pm 1.5% in transverse direction ¹⁵²		15 \pm 1.5% in longitudinal direction ¹⁵² 19 \pm 1.5% in transverse direction ¹⁵²	

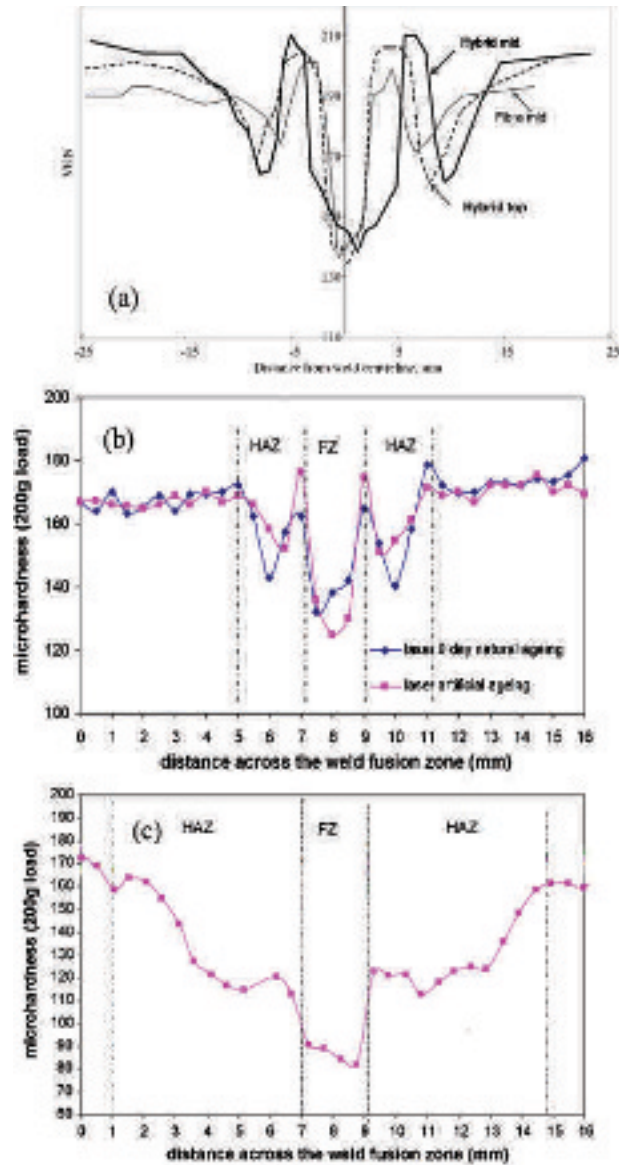


16 Fusion zone microstructures of *a* laser/GMAW hybrid welded AA 7075(T6) aluminium alloy⁴ and *b* laser welded¹⁵¹ (with filler metal) 7xxx series aluminium alloy

the same mechanical properties and microstructural characteristics of the base metal in 7xxx series aluminium alloys without additional heat treatment, such as aging.¹⁵¹ In Fig. 17, the microhardness profiles for 7xxx series aluminium alloy are shown for autogenous Yb fibre laser,¹⁵¹ autogenous Nd:YAG laser,⁴ Yb laser/GMAW hybrid¹⁵¹ and Nd:YAG laser/GMAW⁴ hybrid welding. The results in Fig. 17*a* and *b* are measured after a post-weld heat treatment or aging, and the results shown in Fig. 17*c* are in the as welded condition.^{4,151}

The low hardness of the fusion zone arises from the formation of precipitates and eutectic films along the boundaries of the columnar dendrites in the weld fusion zone, for both laser and hybrid welding.^{4,151} The HAZ hardness is greater than that of the fusion zone but tends to taper off due to precipitate coarsening or phase transformations at high temperatures.⁴ Tensile testing of the 7xxx series aluminium alloy laser and hybrid welds show that the fusion zones for the two welding processes have lower mean tensile strength and ductility than the base metal.^{4,151} The HAZ mechanical properties are significantly better than that of the fusion zone with higher strength and ductility.¹⁵¹

The benefit of the hybrid welding process for the joining of aluminum and magnesium alloys mainly originates from the ability of this process to adjust filler metal additions, heat input, and post heat treatment



17 Microhardness profiles of *a* post-welding heat treated Yb fibre laser and Yb laser/GMAW hybrid,¹⁵¹ *b* aged Nd:YAG laser⁴ and *c* as welded Nd:YAG laser/GMAW hybrid welds based upon the work of Hu and Richardson.⁴ The welds were made on *a* 7xxx series and *b* and *c* AA 7075(T6) aluminium alloys. In *a*, the hybrid weld was evaluated close to the top surface of the weld (hybrid top) and at the mid depth of the weld (hybrid mid). The hardness profiles are functions of the distance across the weld fusion zone and distance from the weld centreline

processes. However, further characterisation and analysis of filler metal and base metal combinations and processing parameters and their effect on weldment structure and mechanical properties is necessary.

Areas for future research

One of the main factors affecting the widespread implementation of laser-arc hybrid welding is the significant initial capital investment required to purchase the laser system. Even with this significant cost barrier, hybrid welding is being applied across a number of different fields, including shipbuilding,⁶⁴ automotive

welding,⁵³ pipelines and railcar industries,¹⁴⁹ primarily in Europe and Asia. Potential expanded application in the joining of important alloys, including stainless steels, advanced high strength steels, titanium and aluminium alloys, will require considerable research, rigorous characterisation and cost analysis. These alloys often require different filler and base metal combinations, which will have to be determined for various hybrid welding conditions in order to obtain optimum weld properties. Significant research also needs to be done to understand the correlation between welding conditions and the resulting weldment structure and properties for each alloy. Detailed characterisation of structure and properties for each alloy remains a major task.

Although hybrid welding has enjoyed growing acceptance in recent years, many important questions about its underlying scientific principles remain unanswered. For example, the laser-arc interactions have been examined by noting increased arc stability and bending of the arc towards the laser generated keyhole.^{1,18,41,56,135} However, the origin of the synergistic interaction that occurs between the arc and laser generated plasmas for various welding conditions is not well understood. Spectroscopic investigations of the optical emissions can provide a better understanding of the laser-arc interactions from the spatial and temporal distributions of electron temperatures and densities in the plasma for various welding conditions. Better understanding of the origins of keyhole stability under the conditions of hybrid welding through experimental and theoretical research would also be useful since the collapse of the keyhole is believed to play an important role in porosity formation in laser welds.

It has been well established that hybrid welding produces welds with desirable widths and depths, but the maximum gap tolerance and weld penetration for various welding conditions have not been quantified. Computational modelling of the heat transfer and fluid flow will enable understanding of the weld pool geometry and cooling rates both within the weld pool and HAZ. In addition, the computed cooling rates at all locations within the weldment can be helpful in understanding the evolution of weld microstructures. Cooling rate data can also help to avoid cracking, brittle phase formation and thermal distortion. Better sensing and process control of the hybrid welding process would also be helpful in expanding its applications.

In summary, expanded use of hybrid welding in applications where high productivity, deep penetration and large gap tolerance are required for a wide variety of engineering alloys is well within the reach of the welding community within a decade. Rigorous studies of relationships between welding conditions and the structure and properties of hybrid welds for important engineering alloys, improved understating of the hybrid welding process through experimental and theoretical investigations and better process control would be helpful in expanding its applications.

References

1. W. M. Steen: *J. Appl. Phys.*, 1980, **51**, 5636–5641.
2. G. Campana, A. Fortunato, A. Ascari, G. Tani and L. Tomesani: *J. Mater. Process. Technol.*, 2007, **191**, 111–113.
3. G. Casalino: *J. Mater. Process. Technol.*, 2007, **191**, 106–110.
4. B. Hu and I. M. Richardson: *Mater. Sci. Eng. A*, 2007, **A459**, 94–100.
5. R. S. Huang, L. M. Liu and G. Song: *Mater. Sci. Eng. A*, 2007, **A447**, 239–243.
6. L. M. Liu, J. F. Wang and G. Song: *Mater. Sci. Eng. A*, 2004, **A381**, 129–133.
7. C. Walz, T. Seefeld and G. Sepold: 'Process stability and design of seam geometry during hybrid welding', Proc. Conf. ICALAO 2001, Jacksonville, FL, USA, October 2001, Laser Institute of America, Paper 305.
8. T. Jokinen, P. Jernstrom, M. Karhu, I. Vanttaja and V. Kujanpaa: 'Optimization of parameters in hybrid welding of aluminum alloy', Proc. 1st Int. Symp. on 'High-power laser macroprocessing', Osaka, Japan, May 2002, Osaka University, 307–312.
9. M. Gao, X. Zeng and Q. W. Hu: *J. Mater. Process. Technol.*, 2007, **184**, 177–183.
10. U. Jasnau, J. Hoffmann and P. Seyffarth: *Robot. Weld. Intell. Autom.*, 2004, **299**, 14–24.
11. A. Mahrle and E. Beyer: *J. Laser Appl.*, 2006, **18**, 169–180.
12. E. A. Metzbowler, P. E. Denney, D. W. Moon, C. R. Feng and S. G. Lambrakos: *Mater. Sci. Forum*, **426–432**, Pt 5, 4147–4152.
13. G. Song, L. M. Liu and P. C. Wang: *Mater. Sci. Eng. A*, 2006, **A429**, 312–319.
14. G. Tani, G. Campana, A. Fortunato and A. Ascari: *Appl. Surf. Sci.*, 2007, **253**, 8050–8053.
15. R. S. Huang, L. M. Liu and F. Zhang: *Chin. Opt. Lett.*, 2008, **6**, 47–50.
16. T. Jokinen, T. Viherva, H. Riikonen and V. Kujanpaa: *J. Laser Appl.*, 2000, **12**, 185–188.
17. C. H. Kim, W. Zhang and T. DebRoy: *J. Appl. Phys.*, 2003, **94**, 2667–2679.
18. L. M. Liu, R. Huang, G. Song and X. Hao: *IEEE Trans. Plasma Sci.*, 2008, **36**, 1937–1943.
19. B. Ribic, R. Rai and T. DebRoy: *Sci. Technol. Weld. Join.*, 2008, **13**, 683–693.
20. M. Gao, X. Zeng, Q. W. Hu and J. Yan: *Sci. Technol. Weld. Join.*, 2008, **13**, 106–113.
21. M. Gao, X. Y. Zeng, J. Yan and Q. W. Hu: *Appl. Surf. Sci.*, 2008, **254**, 5715–5721.
22. P. L. Moore, D. S. Howse and E. R. Wallach: *Sci. Technol. Weld. Join.*, 2004, **9**, 314–322.
23. A. Nonn, W. Dahl and W. Bleck: *Eng. Fract. Mech.*, 2008, **75**, 3251–3263.
24. H. Pinto, A. Pyzalla, H. Hackl and J. Bruckner: *Residual Stresses VII*, 2006, **524–525**, 627–632.
25. J. X. Zhang, Y. Xue and S. L. Gong: *Sci. Technol. Weld. Join.*, 2005, **10**, 643–646.
26. L. Liu, G. Song and J. F. Wang: *Mater. Sci. Forum*, 2005, **488–489**, 361–364.
27. L. M. Liu, G. Song, G. Liang and J. F. Wang: *Mater. Sci. Eng. A*, 2005, **A390**, 76–80.
28. S. Katayama, S. Uchiumi, M. Mizutani, J. Wang and K. Fujii: *Weld. Int.*, 2007, **21**, 25–31.
29. A. Fellman and V. Kujanpaa: *J. Laser Appl.*, 2006, **18**, 12–20.
30. T. Kim, Y. Suga and T. Koike: *JSME Int. J. Ser. A*, 2003, **46A**, 202–207.
31. Y. P. Kim, N. Alam and H. S. Bang: *Sci. Technol. Weld. Join.*, 2006, **11**, 295–307.
32. K. Murakami, Y. Mitooka, M. Hino, H. Iogawa, H. Ono and S. Katayama: *J. Jpn Inst. Met.*, 2006, **70**, 134–137.
33. G. L. Qin, Z. Lei and S. Y. Lin: *Sci. Technol. Weld. Join.*, 2007, **12**, 79–86.
34. P. T. Swanson, C. J. Page, E. Read and H. Z. Wu: *Sci. Technol. Weld. Join.*, 2007, **12**, 153–160.
35. Anonymous: *Weld. J.*, 2002, **81**, 58–58.
36. Anonymous: *Ind. Robot*, 2002, **29**, 170–171.
37. O. E. Canyurt, H. R. Kim and K. Y. Lee: *Mech. Mater.*, 2008, **40**, 825–831.
38. C. Kim, W. Choi, J. Kim and S. Rhee: *Mater. Trans.*, 2008, **49**, 179–186.
39. H. R. Kim, Y. W. Park and K. Y. Lee: *Sci. Technol. Weld. Join.*, 2008, **13**, 312–317.
40. G. A. Turichin, A. M. Grigor'ev, E. V. Zemlyakov, E. A. Valdaitseva, U. Dilthey and A. Gumeniuk: *High Temp.*, 2006, **44**, 647–655.
41. C. Bagger and F. O. Olsen: *J. Laser Appl.*, 2004, **17**, 2–14.
42. M. Kutsuna and L. Chen: 'Interaction of both plasmas in CO₂ laser-MAG hybrid welding of carbon steel', Proc. 1st Int. Symp. on 'High-power laser macroprocessing', Osaka, Japan, May 2002, Osaka University, 341–346.
43. M. Wouters, J. Powell and A. F. H. Kaplan: *J. Laser Appl.*, 2006, **18**, 181–184.

44. Y. Yao, M. Wouters, J. Powell, K. Nilsson and A. F. H. Kaplan: *J. Laser Appl.*, 2006, **18**, 283–288.
45. H. Staufner: *Weld. J.*, 2007, **86**, 36–40.
46. Anonymous: *Adv. Mater. Processes*, 2007, **165**, 23–23.
47. J. F. Coutouly, P. Deprez, J. Demonchaux and A. I. Koruk: *Lasers Eng.*, 2006, **16**, 399–411.
48. C. Y. Song, Y. W. Park, H. R. Kim, K. Y. Lee and J. Lee: *Proc. Inst. Mech. Eng. B, J. Eng. Manuf.*, 2008, **222B**, 507–518.
49. L. Liu, X. Hao and G. Song: *Mater. Trans.*, 2006, **47**, 1611–1614.
50. B. Hu and G. den Ouden: *Sci. Technol. Weld. Join.*, 2005, **10**, 76–81.
51. C. J. Page, T. Devermann, J. Biffin and N. Blundell: *Sci. Technol. Weld. Join.*, 2002, **7**, 1–10.
52. S. M. Joo, Y. P. Kim, C. S. Ro, H. S. Bang and J. U. Park: *Adv. Nondestr. Eval.*, 2004, **270–273**, Pt 1–3, 2383–2388.
53. T. Graf and H. Staufner: *Weld. J.*, 2003, **82**, 42–48.
54. M. Ono, Y. Shinbo, A. Yoshitake and M. Ohmura: ‘Welding properties of thin steel sheets by laser-arc hybrid welding: laser-focused arc welding’, Proc. 1st Int. Symp. on ‘High-power laser macroprocessing’, Osaka, Japan, May 2002, Osaka University, 369–374.
55. G. Song, L. M. Liu, M. S. Chi and J. F. Wang: *Mater. Sci. Forum*, 2005, **488–489**, 371–375.
56. Y. B. Chen, Z. L. Lei and L. Wu: *Sci. Technol. Weld. Join.*, 2006, **11**, 403–411.
57. S. A. David, T. DebRoy and J. M. Vitek: *MRS Bull.*, 1994, **19**, 29–35.
58. T. DebRoy and S. A. David: *Rev. Mod. Phys.*, 1995, **67**, 85–112.
59. S. Mishra and T. DebRoy: *Mater. Sci. Technol.*, 2006, **22**, 253–278.
60. H. Zhao, D. R. White and T. Debroy: *Int. Mater. Rev.*, 1999, **44**, 238–266.
61. S. Mishra and T. DebRoy: *Acta Mater.*, 2004, **52**, 1183–1192.
62. S. Kou: ‘Welding metallurgy’, 13–62; 2003, New York, John Wiley & Sons.
63. J. F. Lancaster: ‘The physics of welding’, 9–29; 1986, New York, Pergamon Press.
64. S. Herbert: *Weld. J.*, 2004, **83**, 39–43.
65. R. Rai, G. G. Roy and T. DebRoy: *J. Appl. Phys.*, 2007, **101**, 054909.
66. R. Rai, J. W. Elmer, T. A. Palmer and T. DebRoy: *J. Phys. D*, 2007, **40D**, 5753–5766.
67. R. Rai, S. M. Kelly, R. P. Martukanitz and T. DebRoy: *Metall. Mater. Trans. A*, 2008, **39A**, 98–112.
68. A. De and T. DebRoy: *Weld. J.*, 2005, **84**, 101s–112s.
69. H. Zhao and T. Debroy: *Metall. Mater. Trans. B*, 2001, **32**, 163–172.
70. S. A. David and T. Debroy: *Science*, 1992, **257**, 497–502.
71. W. W. Duley: ‘CO₂ lasers effects and applications’, 1976, San Diego, CA, Academic Press.
72. G. S. Arnold: *Appl. Opt.*, 1984, **23**, 1434–1436.
73. S. B. Boyden and Y. W. Zhang: *J. Thermophys. Heat Transfer*, 2006, **20**, 9–15.
74. J. Greses, P. A. Hilton, C. Y. Barlow and W. M. Steen: *J. Laser Appl.*, 2004, **16**, 9–15.
75. W. W. Duley: ‘Laser processing and analysis of materials’, 1983, New York, Plenum Press.
76. M. von Allmen: ‘Laser-beam interactions with materials’, 1987, New York, Springer-Verlag.
77. X. Z. Jin, L. J. Li and Y. Zhang: *J. Phys. D*, 2002, **35D**, 2304–2310.
78. T. P. Hughes: ‘Plasmas and laser light’, 1975, New York, John Wiley & Sons.
79. R. G. Lerner and G. L. Trigg: ‘Encyclopedia of physics’, 1991, New York, VCH Publishers.
80. C. J. Nonhof: ‘Material processing with Nd-lasers’, 1988, Ayr, Electrochemical Publications Limited.
81. S. Pfalzner and P. Gibbon: *Phys. Rev. E*, 1998, **57E**, 4698–4705.
82. G. Xu, Z. Cheng, J. Xia, X. Li and J. Jiang: ‘Laser keyhole welding on aluminum alloys’, Proc. 1st Int. Symp. on ‘High-power lasers in manufacturing’, Osaka, Japan, May 2000, Osaka University, 710–716.
83. J. Mazumder: ‘Laser-beam welding’, in ‘ASM handbook’, Vol. 6, ‘Welding, brazing, and soldering’, (ed. F. Reidenbach), 262–269; 1993, Materials Park, OH, ASM International.
84. J. H. Cho and S. J. Na: *J. Phys. D*, 2006, **39D**, 5372–5378.
85. W. Zhang: ‘Probing heat transfer, fluid flow and microstructural evolution during fusion welding of alloys’, PhD thesis, Pennsylvania State University, University Park, PA, USA, 2004.
86. P. Sahoo, T. DebRoy and M. J. McNallan: *Metall. Trans. B*, 1988, **19B**, 483–491.
87. D. A. Schauer, W. H. Giedt and S. M. Shintaku: *Weld. J.*, 1978, **57**, S127–S133.
88. J. D. Jackson: ‘Classical electrodynamics’, 1998, New York, John Wiley & Sons.
89. K. Mundra, T. DebRoy and K. M. Kelkar: *Numer. Heat Transfer A*, 1996, **29A**, 115–129.
90. R. T. C. Choo and J. Szekely: *Weld. J.*, 1991, **70**, S223–S233.
91. G. M. Oreper and J. Szekely: *Metall. Trans. A*, 1987, **18A**, 1325–1332.
92. W. Zhang, G. G. Roy, J. W. Elmer and T. DebRoy: *J. Appl. Phys.*, 2003, **93**, 3022–3033.
93. B. E. Launder and D. B. Spalding: ‘Lectures in mathematical model of turbulence’, 1972, London, Academic Press.
94. D. C. Wilcox: ‘Turbulence modeling for CFD’, 1993, La Cañada, CA, DCW Industries.
95. T. DebRoy and A. K. Majumdar: *J. Met.*, 1981, **33**, (11), 42–47.
96. M. El Rayes, C. Walz and G. Sepold: *Weld. J.*, 2004, **83**, 147s–153s.
97. L. M. Liu and X. Zhao: *Mater. Charact.*, 2008, **59**, 1279–1284.
98. H. Zhao and T. Debroy: *J. Appl. Phys.*, 2003, **93**, 10089–10096.
99. Y. Naito, M. Mizutani and S. Katayama: *J. Laser Appl.*, 2006, **18**, 21–27.
100. J. Kroos, U. Gratzke and G. Simon: *J. Phys. D*, 1993, **26D**, 474–480.
101. V. Semak and A. Matsunawa: *J. Phys. D*, 1997, **30D**, 2541–2552.
102. T. Klein, M. Vicanek, J. Kroos, I. Decker and G. Simon: *J. Phys. D*, 1994, **27D**, 2023–2030.
103. P. A. A. Khan and T. DebRoy: *Metall. Trans. B*, 1984, **15B**, 641–644.
104. D. R. Poirier and G. H. Geiger: ‘Transport phenomena in materials processing’, 1994, Warrendale, PA, The Minerals, Metals, and Materials Society.
105. J. Kroos, U. Gratzke, M. Vicanek and G. Simon: *J. Phys. D*, 1993, **26D**, 481–486.
106. S. Tsukamoto, I. Kawaguchi, G. Arakane and H. Honda: ‘Keyhole behavior in high power laser welding’, Proc. 1st Int. Symp. on ‘High-power laser macroprocessing’, Osaka, Japan, May 2002, Osaka University, 251–256.
107. P. Solana and J. L. Ocana: *J. Phys. D*, 1997, **30D**, 1300–1313.
108. J. Tusek and M. Suban: *Sci. Technol. Weld. Join.*, 1999, **4**, 308–311.
109. P. Seyffarth: ‘Laser-arc processes and their applications in welding and material treatment’, 2002, London, Taylor & Francis.
110. G. J. Dunn and T. W. Eager: *Metall. Trans. A*, 1986, **17**, 1865–1871.
111. S. Akbar and K. Etemadi: *Plasma Chem. Plasma Process.*, 1997, **17**, 251–262.
112. K. C. Hsu, K. Etemadi and E. Pfender: *J. Appl. Phys.*, 1982, **54**, 1293–1301.
113. N. S. Tsai and T. W. Eager: *Metall. Trans. B*, 1985, **16B**, 841–846.
114. H. B. Cary and S. C. Helzer: ‘Modern welding technology’, 2005, Upper Saddle River, NJ, Pearson Education.
115. M. A. Uman: ‘Introduction to plasma physics’, 1–7; 1964, New York, McGraw-Hill.
116. F. F. Chen: ‘Introduction to plasma physics and controlled fusion’, Vol. I, ‘Plasma physics’, 3–7; 1984, New York, Plenum Press.
117. A. B. Cambel: ‘Plasma physics and magnetofluidmechanics’, 1963, New York, McGraw-Hill.
118. A. B. Murphy: *J. Phys. D*, 2001, **34**, R151–R173.
119. H. R. Griem: ‘Plasma spectroscopy’, 1964, New York, McGraw-Hill.
120. F. Cabannes and J. Chapelle: ‘Spectroscopic plasma diagnostics’, 367–469; 1971, New York, Wiley InterScience.
121. P. W. J. M. Boumans: ‘Theory of spectrochemical excitation’, 79–88; 1966, New York, Plenum Press.
122. T. A. Palmer and T. DebRoy: *Metall. Mater. Trans. B*, 2000, **31B**, 1371–1385.
123. T. A. Palmer and T. DebRoy: *Sci. Technol. Weld. Join.*, 1998, **3**, 190–203.
124. M. Pastor, H. Zhao, R. P. Martukanitz and T. DebRoy: *Weld. J.*, 1999, **78**, 207S–216S.
125. X. He, T. DebRoy and P. W. Fuerschbach: *J. Appl. Phys.*, 2003, **94**, 6949–6958.
126. G. N. Haddad and A. J. D. Farmer: *Weld. J.*, 1985, **64**, S399–S342.
127. A. E. F. Gick, M. B. C. Quigley and P. H. Richards: *J. Phys. D*, 1973, **6D**, 1941–1949.

128. C. Fanara and I. M. Richardson: *J. Phys. D*, 2001, **34D**, 2715–2725.
129. K. S. Drellishak, D. P. Aeschlim and A. B. Cambel: *Phys. Fluids*, 1965, **8**, 1590–1600.
130. K. S. Drellishak, C. F. Knopp and A. B. Cambel: *Phys. Fluids*, 1963, **6**, 1280–1288.
131. R. Miller and T. DebRoy: *J. Appl. Phys.*, 1990, **68**, 2045–2050.
132. M. M. Collur and T. DebRoy: *Metall. Trans. B*, 1989, **20B**, 277–286.
133. B. Hu and G. den Ouden: *Sci. Technol. Weld. Join.*, 2005, **10**, 427–431.
134. P. Sahoo, M. M. Collur and T. DebRoy: *Metall. Trans. B-Process Metall.*, 1988, **19**, 967–972.
135. Y. Naito, S. Katayama and A. Matsunawa: 'Keyhole behavior and liquid flow in molten pool during laser-arc hybrid welding', Proc. 1st Int. Symp. on 'High-power laser macroprocessing', Osaka, Japan, May 2002, Osaka University, 357–362.
136. R. W. Messler: *Weld. J.*, 2004, **83**, 30–34.
137. G. Y. Zhao, M. Dassanavake and K. Etemadi: *Plasma Chem. Plasma Process.*, 1990, **10**, 87–98.
138. X. Zhou and J. Herberlein: *J. Phys. D*, 1998, **31D**, 2577–2590.
139. J. Wang, K. Kusumoto and K. Nezu: *Sci. Technol. Weld. Join.*, 2004, **9**, 369–373.
140. M. Gao, X. Y. Zeng and Q. W. Hu: *Sci. Technol. Weld. Join.*, 2006, **11**, 517–522.
141. J. Zhou, W. H. Zhang, H. L. Tsai, S. P. Martin, P. C. Wang and R. Menassa: 'Modeling the transport phenomena during hybrid laser-MIG welding process', Proc. ASME Int. Mechanical Engineering Cong. and Expos., Washington, DC, USA, November 2003, ASME.
142. J. Zhou and H. L. Tsai: *Int. J. Heat Mass Transfer*, 2008, **51**, 4353–4366.
143. J. Dowden and P. Kapadia: *J. Phys. D*, 1995, **28D**, 2252–2261.
144. Y. B. Chen, L. Q. Li, J. F. Fang and X. S. Feng: *J. Mater. Sci. Technol.*, 2003, **19**, 23–26.
145. E. W. Reutzel, M. J. Sullivan and D. A. Mikesic: *Weld. J.*, 2006, **85**, 66–71.
146. H. Zhao and T. DebRoy: *Weld. J.*, 2001, **80**, 204s–210s.
147. M. Ono, Y. Shinbo, A. Yoshitake and M. Ohmura: *NKK Tech. Rev.*, 2002, **86**, 8–12.
148. W. H. Zhang, J. Zhou and H. L. Tsai: 'Numerical modeling of keyhole dynamics in laser welding', Proc. 1st Int. Symp. on 'High-power laser macroprocessing', Osaka, Japan, May 2002, Osaka University, 180–185.
149. J. Defalco: *Weld. J.*, 2007, **86**, 47–51.
150. B. Hu and I. M. Richardson: *Mater. Sci. Eng. A*, 2006, **A429**, 287–294.
151. C. M. Allen, G. Verhaeghe, P. A. Hilton, C. P. Heason and P. B. Prangnell: *Mater. Sci. Forum*, 2006, **519–521**, 1139–1144.
152. R. S. Coelho, A. Kostka, H. Pinto, S. Riekehr, M. Kocak and A. R. Pyzalla: *Mater. Sci. Eng. A*, 2008, **A485**, 20–30.
153. M. Shome: *Mater. Sci. Eng. A*, 2007, **A445**, 454–460.
154. L. M. Liu, G. Song, J. F. Wang and G. L. Liang: *Trans. Nonferr. Met. Soc. China*, 2004, **14**, 550–555.
155. T. W. Kim, J. C. Kim, Y. Hasegawa and Y. Suga: *Des. Process. Prop. Adv. Eng. Mater.*, 2004, **449–4**, Pts 1 and 2, 417–420.
156. L. M. Liu, X. J. Liu and S. H. Liu: *Scr. Mater.*, 2006, **55**, 383–386.
157. L. M. Liu, G. Song and M. S. Chi: *Mater. Sci. Technol.*, 2005, **21**, 1078–1082.
158. Z. D. Zhang, L. M. Liu, Y. Shen and L. Wang: *Mater. Charact.*, 2008, **59**, 40–46.
159. A. De and T. DebRoy: *J. Appl. Phys.*, 2004, **95**, 5230–5240.
160. A. De and T. DebRoy: *J. Phys D; Appl. Phys.*, 2004, **37**, 140–150.